

International
Progress Report

IPR-07-12

Äspö Hard Rock Laboratory

Prototype Repository

Acoustic emission and ultrasonic
monitoring results from deposition
hole DA3545G01 in the Prototype
Repository between October 2006
and March 2007

F. Zolezzi
J.R. Haycox
W.S. Pettitt
Applied Seismology Consultants

August 2007

Svensk Kärnbränslehantering AB

Swedish Nuclear Fuel
and Waste Management Co
Box 5864
SE-102 40 Stockholm Sweden
Tel 08-459 84 00
+46 8 459 84 00
Fax 08-661 57 19
+46 8 661 57 19



**Äspö Hard Rock
Laboratory**

Report no.	No.
IPR-07-12	F63K
Author	Date
F. Zolezzi	August 2007
J.R. Haycox	
W.S. Pettitt	
Checked by	Date
Lars-Erik Johannesson	2007-10-29
R.P. Young	
Approved	Date
Anders Sjöland	2007-11-05

Äspö Hard Rock Laboratory

Prototype Repository

Acoustic emission and ultrasonic monitoring results from deposition hole DA3545G01 in the Prototype Repository between October 2006 and March 2007

F. Zolezzi
J.R. Haycox
W.S. Pettitt
Applied Seismology Consultants

August 2007

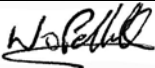
Keywords: Field test, Prototype Repository, Acoustic emission, Ultrasonic monitoring, P-wave velocity, S-wave velocity, Rock fractures, Rock properties

This report concerns a study which was conducted for SKB. The conclusions and viewpoints presented in the report are those of the author(s) and do not necessarily coincide with those of the client.

Report DLV-07-08

**To
SKB**

APPLIED SEISMOLOGY CONSULTANTS

Last Edited	12 October 2007
File name	SKBProto_Sep06Mar07_02082007.doc
Last Printed	12 October 2007
Signature	

Executive summary

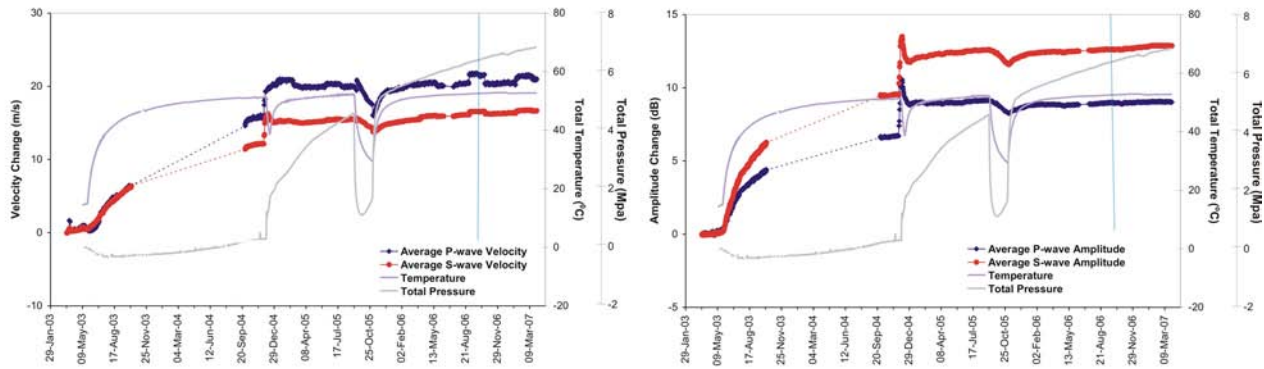
This report describes results from acoustic emission (AE) and ultrasonic monitoring around a canister deposition hole (DA3545G01) in the Prototype Repository Experiment at SKB's Hard Rock Laboratory (HRL), Sweden. The experiment has been designed to simulate a disposal tunnel in a real deep repository for removal of high-level radioactive waste.

The test consists of a 90m long, 5m diameter sub-horizontal tunnel excavated in dioritic granite and the monitoring aims to examine changes in the rock mass caused by an experimental repository environment, in particular due to thermal stresses induced from canister heating and pore pressures induced from tunnel sealing.

Two techniques are utilised here to investigate the processes occurring within the rock mass around the deposition hole: ultrasonic survey and acoustic emission (AE). Ultrasonic surveys are used to 'actively' examine the rock. Velocity changes are measured between transmitter-receiver pairs using a cross-correlation technique that allows a velocity resolution of $\pm 2 \text{ m.s}^{-1}$. Amplitude and velocity changes on the ray paths can then be interpreted in terms of changes in the material properties of the rock. Calculations using the velocities can determine the changes in dynamic moduli, Young's modulus and Poisson's ratio, to give direct indications of the properties of the rock through which the raypaths travel. Crack density and saturation can also be calculated to determine changes in crack properties in the damaged and disturbed zones. AE monitoring is a 'passive' technique similar to earthquake monitoring but on a much smaller distance scale (source dimensions of millimetres). AEs occur on fractures in the rock when they are created or when they move.

This report relates to the period between 1st October 2006 and 31st March 2007, and is the fourth of a 6-monthly processing and interpretation of the results for the experiment. Ultrasonic monitoring has been conducted at the Prototype Repository since September 1999. During excavation, monitoring of both deposition holes in section 2 was undertaken to delineate zones of stress related fracturing and quantitatively measure fracturing in the damaged zone. A permanent ultrasonic array was installed in the rock mass in June 2002 around deposition hole DA3545G01.

During this monitoring period, very little change in P- or S-wave velocity is observed. Temporal jumps, of 1 m.s^{-1} or less, in velocity occur in October, January and March. These changes are of interest but are much smaller than the estimated uncertainties in the technique. P-wave and S-wave amplitudes decrease in October, but exhibit a relatively constant increase during this monitoring period with S-waves increasing to a greater extent. P-wave amplitude results vary more by raypath than S-waves. Raypaths have been categorised following spatial criteria presented in previous reporting periods. The amplitude for category 'C1' does not increase after the initial drop in October. Similarly, category 'S1' also exhibits little change, ending the monitoring period at approximately the same amplitude as at the start. The biggest amplitude increases are observed in categories 'C2' and 'Far'. For all raypaths examined, the variations observed for both P- and S-wave amplitudes and velocities are very small indicating a stable rock mass.

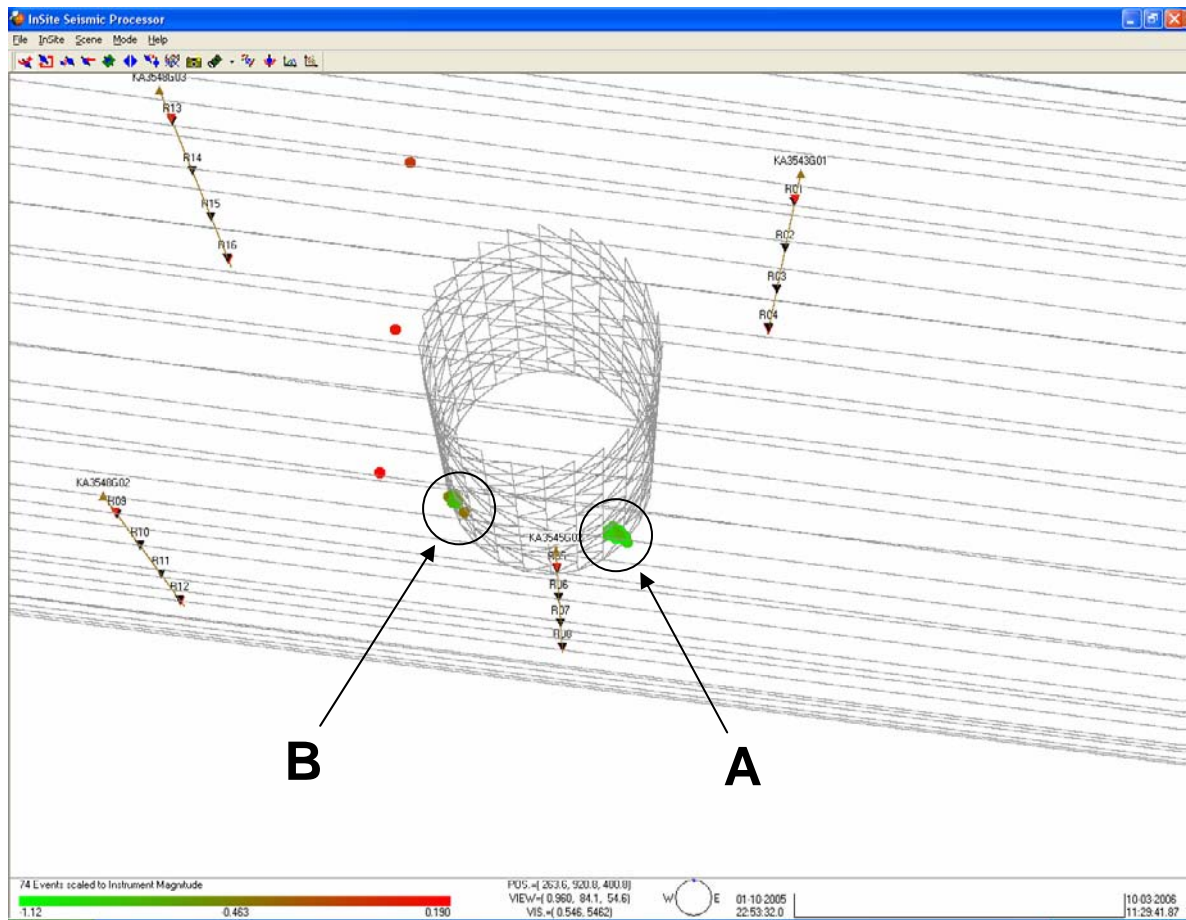


Average velocity change and amplitude change. The blue line show the start of the period analysed in this report (Oct. 06 – March 07).

Changes in Young's Modulus, Poisson's Ratio, Crack Density and Saturation Parameters have been calculated from the average measured velocities for different raypath categories. Young's Modulus, Poisson's ratio and saturation are observed to decrease in October, remain almost constant until January when an increase is observed, then decrease again in March. All raypath categories exhibit similar changes during this monitoring period. Crack density shows the opposite behaviour displaying an increase in October, followed by a decrease in January, and an increase in March. This trend is observed for all the raypaths passing through the region of low compressive or tensile stress, and through a possible region of tensile fracturing. Overall during the monitoring period, the velocity and amplitude results have shown that the rock mass around the deposition hole has not altered significantly. Gradual increases in temperature and pressure have led to a slow stiffening of the rock, alongside a similarly slow reduction in crack density. During a relatively stable period of environmental characteristics, no dramatic changes in the rock mass have been measured.

During the six-month period, 74 AEs have been located with high confidence from 83 triggered events. The rate of triggers remains reasonably constant. On average, 0.4 triggers were recorded per day. An average of 0.20 events is located per day. Study of the spatial distribution of AEs shows 54 of the 74 located events locate in a very tight cluster at a depth of 455.1 m to the south east, while another 17 events are located in a smaller cluster at a depth of 455.0 m in the south-west side of deposition hole DA3545G01. The first cluster (A) locates in a region of low-compressive or tensile stresses. The second cluster (B) is located in a region high compressive stresses. Events in the clusters are located close enough together to be considered occurring on the same feature and occur over the whole reporting period with no significant peaks in activity. AEs may be occurring at this position due to the presence of pre-existing microcracks, generated during excavation. Similar clustering was observed in the previous monitoring period [Haycox *et al.*, 2006b]. A brief study has been conducted to determine whether the event clusters could be caused by movement of one of the many geomechanical instruments placed in the deposition hole for monitoring purposes. This possibility has been discarded as no instruments are positioned at the correct height, or orientation with respect to the deposition hole axis. The AEs are characterized by relatively very low magnitudes ($-1.12 < \text{Instrument Magnitude} < 0.190$), which means that the clusters do not represent significant activity.

The number of events in the general rock mass are relatively low and therefore indicate the rock around the deposition holes has remained stable during this six-month period. This result is consistent with what would be expected from a relatively constant pressure and temperature environment during the study period.



Clusters (defined 'A' and 'B') of AE activity observed on the South side of deposition hole DA3545G01.

Sammanfattning

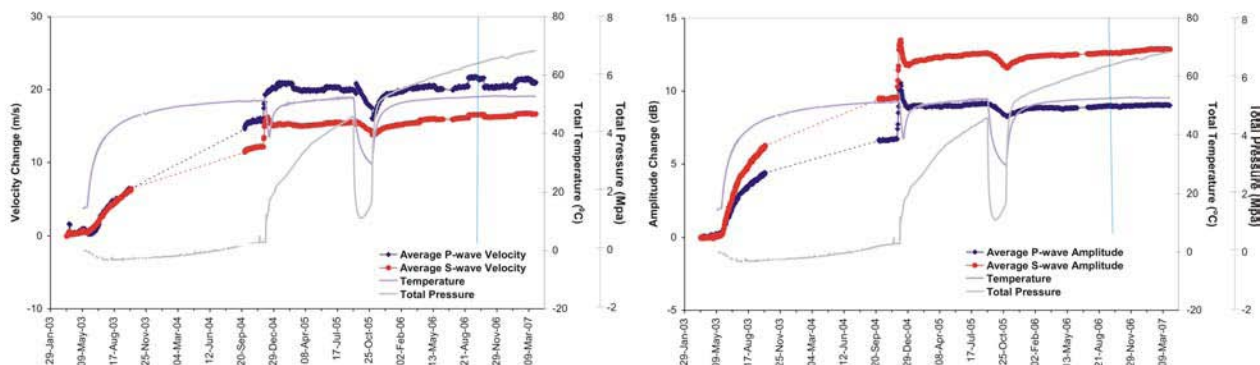
Denna rapport beskriver resultaten från AE-mätningar och ultaljudsmätningar runt deponeringshål DA3545G01 i prototypförvaret vid SKB:s Hard Rock Laboratory. Experimentet har designats för att simulera en deponeringstunnel i ett verkligt djupförvar för högaktivt radioaktivt avfall.

Försöket består av en 90 m lång horisontell tunnel med en diameter på 5 m, uttagen ur en dioritisk granit. Syftet med mätningen är att undersöka förändringar i bergmassan som orsakats av en experimentell förvarsmiljö, speciellt med avseende på värmespanning från uppvärmning av kapseln och portryck orsakade av förseglingen av tunneln.

Två tekniker används för att undersöka de processer som inträffar i bergmassan runt deponeringshålet; ultraljudsmätning och AE-övervakning. Ultraljudsmätning används för att "aktivt" undersöka berget. Hastighetsförändringar mäts mellan sändare - givare par genom att använda en kors-korrelationsteknik som möjliggör en mätnoggrannhet på $\pm 2 \text{ m.s}^{-1}$. Förändringar i amplitud och hastighet hos signalen när den passerat genom bergmassan i olika signalvägar relativt deponeringshålen, ("ray path") har sedan använts för att undersöka förändringar i bergegenskaperna. Hastigheterna användas för att bestämma förändringar i dynamisk modul, elasticitetsmodul och tvärkontraktionstal som ger direkta indikationer på egenskaperna på berget genom vilket vågen passerar. Sprickdensitet och vattenmättnadsgrad kan också beräknas för att fastställa förändringar i sprickornas egenskaper i den skadade och störda zonen. AE-övervakning är en 'passiv' teknik som liknar jordbävningsovervakning men på en mycket mindre avståndsskala (källdimensioner på millimetrar). AE (Acoustic Emission) uppkommer hos bergsprickor när de bildas eller när de rör sig

Denna rapport hänför sig till mätningar under perioden 1 oktober, 2006 till 31 mars, 2007 och är den fjärde rapporten med processning och tolkning av data från testerna. Ultraljudsmätningar har utförts i projektet Prototype Repository sedan september 1999. Mätningar gjordes runt de båda deponeringshålen i sektion 2 under borringen av hålen. Syftet med dessa mätningar var att beskriva zoner med spänningsrelaterade sprickor och kvantitativt mäta sprickutbildningen i den störda zonen runt deponeringshålen. Ett permanent ultraljudssystem installerades i berget runt deponeringshål DA3545G01 i juni 2002.

Mycket små förändringar i hastigheten hos P- och S-vågorna uppmättes under denna mätperiod. Temporära hopp på 1 m.s^{-1} eller mindre förekom under oktober, januari och mars. Dessa förändringar är intressanta men är mycket mindre än den uppskattade osäkerheten hos den använda tekniken. Amplituderna på P- och S-vågorna minskar under oktober, men visar en relativt konstant ökning under mätperioden i sin helhet, S-vågorna ökar mest. P-vågens amplitud varierar mer med signalvägen (ray path) än vad S-vågen gör. Signalvägarna har kategoriserats på samma sätt som för tidigare rapporteringsperioder. Amplituden för kategori "C1" ökar inte efter den inledande minskningen under oktober. På liknande sätt uppvisar kategori "S1" också små förändringar och slutar mätperioden på ungefär samma amplitud som vid början av perioden. Den största amplitudökning observeras för kategorin "C2" och "Far". Variationen i P- och S-vågens amplituder och hastigheter är små för samliga undersökta signalvägar vilket indikerar att bergmassan är stabil.

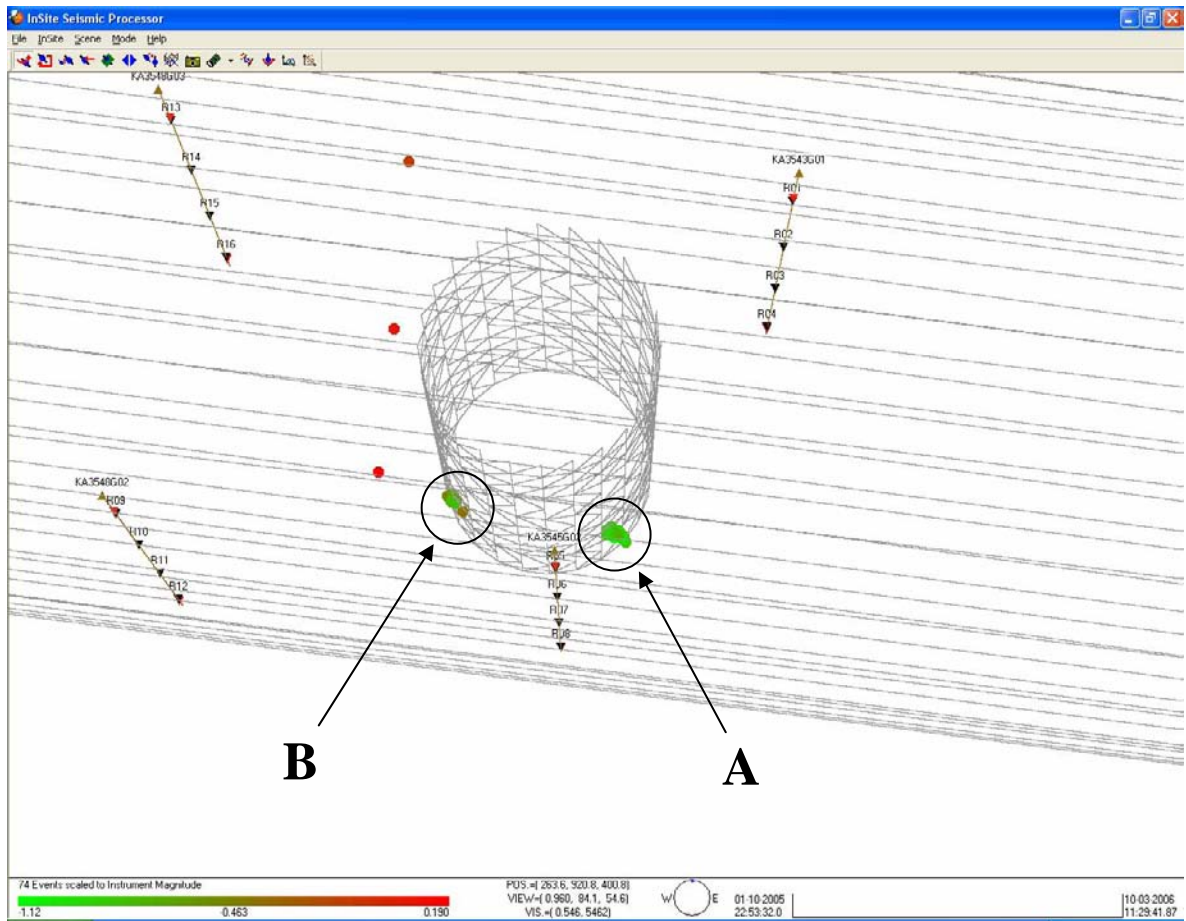


Medelhastighets- och amplitudförändring. Den vertikala blå linjen anger starten på perioden som analyseras i denna rapport (oktober 2006 - mars 2007).

Förändringar i E-modul, tvärkontraktionstal, sprickdensitet och vattenmättnadsgrad har beräknats med hjälp av medelhastigheter för olika kategorier av signalvägar. E-modulen, tvärkontraktionstalet och vattenmättnadsgrad minskar under oktober, förblir konstanta till januari då en ökning observeras och sedan en minskning igen i mars. Alla kategorier av signalvägar visar likartade förändringar under mätperioden. Sprickdensiteten uppvisar ett motsatt förlopp, en ökning i oktober, följd av en minskning i januari och en ökning i mars. Denna trend är observerad för alla signalvägar som går genom regioner med låga kompressionsspänningar eller dragspänningar och genom regioner med eventuella dragsprickor. Generellt har mätningarna av hastighet och amplitud under denna sexmånadersperiod visat att bergvolymen runt deponeringshållet inte förändrats signifikant. En gradvis ökning av temperatur och tryck har lett till en långsam ökning av bergets styvhet samtidigt med en minskning i mängden sprickor. Under en period med relativt stabila förhållanden har inga dramatiska förändringar i bergmassan observerats.

Under sexmånadsperioden har 74 akustiska utstrålningar (**A**coustic **E**mision) lokaliserats med stor säkerhet mha 83 ”triggade” händelser. I medeltal registrerades 0,4 ”triggade” händelser per dag och 0,2 händelser lokaliserades per dag i medeltal. Studie av den rumsliga fördelningen av AE visar att 54 av de 74 lokaliserade händelserna ligger i ett mycket tätt kluster på djupet 455.1 m åt sydost, medan ytterligare 17 händelser är lokaliserade i ett litet kluster på ett djup av 455.0 m på sydvästra sidan av deponeringshållet DA3545G01. Det första klustret (A) ligger i en region med låga kompressionsspänningar eller dragspänningar. Det andra klustret (B) ligger i en region med höga kompressionsspänningar. Händelserna ligger så nära varandra så de kan anses ha uppstått vid samma diskontinuitet och de inträffar under hela rapporteringsperioden utan några pikar i aktivitet. AE kan ha inträffat i detta läge p.g.a. förekomst av tidigare, under uttaget av berget uppkomna mikrosprickor. Liknande kluster observerades under den föregående mätperioden. En omfattande undersökning har gjorts för att utreda om kluster av händelser kunde ha orsakats av rörelser av en av de geomekaniska instrument som placerats i deponeringshållet. Denna möjlighet har uteslutits eftersom inga instrument är placerade på rätt höjd eller orientering i förhållande till deponeringshållets axel. De registrerade AE har relativt liten magnitud ($-1.12 < \text{Instrument Magnitud} < 0.190$) vilket betyder att kluster inte representerar en signifikant aktivitet.

Antalet händelser i bergmassan är relativt få och indikerar därför att bergvolymen runt deponeringshålen har förblivit stabil under denna sexmånadersperiod. Detta resultat är konsistent med vad som kan förväntas vid en miljö med ett relativt konstant tryck och temperatur.



Kluster ('A' and 'B') av AE aktiviteter observerade på södra sidan av deponeringshålet DA3545G01.

Contents

Executive summary	5
Sammanfattning	9
Contents	13
Table of Figures	15
Table of Tables	18
1 Introduction	19
2 Specific Objectives	21
3 Results	23
3.1 Ultrasonic surveys	23
3.2 Acoustic Emissions	35
4 Conclusions	45
4.1 Monitoring Between October 2006 and March 2007	45
4.2 Summary of Monitoring from the Heating and Pressurisation Phase	47
4.3 Recommendations	47
References	61
Appendix I Previous Monitoring at the Prototype Repository	63
Appendix II Methodology	65
Appendix III Processing Parameters	73

Table of Figures

Figure 1-1: Plan view of the experimental tunnels at the Äspö HRL and the location of the Prototype Repository. A schematic illustration of the final experimental set up is shown with canisters and bentonite clay buffer installed in the 1.75m diameter deposition holes. Note the entrance of the tunnel is towards the left. Graphics are modified from SKB[1999].	19
Figure 3-1: Temperature around deposition hole DA3545G01. The sensors are positioned mid-way up the deposition hole with different depths into the rock mass (see right-hand inset) [Goudarzi, 2007].	23
Figure 3-2: Total pressure in (a) the backfill over deposition hole DA3545G01; and (b) in the rock adjacent to deposition hole DA3545G01 [Goudarzi, 2007]. The position of the sensor is presented in the figure legend as distance down, angle around and distance from the axis of the deposition.	25
Figure 3-3: Average P- and S- wave (A) velocity change and (B) amplitude change, for the reporting period. Temperature (TR6045) and total pressure (PB616) are displayed on the secondary axes. Chart (A') is a different scale plot of chart (A) just to show changing in temperatures.	26
Figure 3-4: Example plots of (a) raw waveform data points and (b) cross correlation windows for the raypath transmitter 5 to receiver 13 on 18 th October and 20 th October 2007. The second plot shows the reference survey from 8 th December 2004.	27
Figure 3-5: Interpretation of the ultrasonic results during excavation in terms of disturbed and damaged regions around the deposition hole. Zones of induced stress are inferred from elastic modelling and the σ_1 orientation. After Pettitt <i>et al.</i> [1999].	29
Figure 3-6: Velocity changes measured on ray path category 'S3' (Figure 3-5) for deposition hole DA3545G01. Ray paths shown are from a <i>top</i> transmitter to receivers with increasing depth: a) transmitter, $t_n=1$, receiver, $r_n=5$; b) $t_n=1$, $r_n=6$; c) $t_n=1$, $r_n=7$; d) $t_n=4$, $r_n=1$. Schematic diagrams in the right margin indicate the relative positions of transmitter (red) and receiver (gold). Temperature (TR6045) is displayed on the secondary axes.	30
Figure 3-7: Velocity changes measured on ray path category 'S1' (Figure 3-5) for deposition hole DA3545G01. Ray paths shown are from a <i>top</i> transmitter to receivers with increasing depth: a) transmitter, $t_n=7$, receiver, $r_n=5$; b) $t_n=7$, $r_n=6$; c) $t_n=7$, $r_n=7$; d) $t_n=7$, $r_n=8$. Schematic diagrams in the right margin indicate the relative positions of transmitter (red) and receiver (gold). Temperature (TR6045) is displayed on the secondary axes.	31
Figure 3-8: Velocity change plots of 5 raypath categories around deposition hole DA3545G01 for (a) P-waves and (b) S-waves. Temperature (TR6045) and total pressure (PB616) are displayed on the secondary axes.	32
Figure 3-9: Amplitude change plots of 5 raypath categories around deposition hole DA3545G01 for (a) P-waves and (b) S-waves. Temperature (TR6045) and total pressure (PB616) are displayed on the secondary axes.	33

Figure 3-10: Changes in rock parameters during this reporting period for average P- and S-wave velocity values on different raypath orientations. (a) Young’s Modulus, (b) Poisson’s Ratio, (c) Crack Density and (d) Saturation. Raypath orientations are described in Figure 3-5. Temperature (TR6045) and total pressure (PB616) are displayed on the secondary axes.	34
Figure 3-11: Temporal response plot of (a) AE triggers and (b) located AEs; number per day on left axes and cumulative number right hand axes.	38
Figure 3-12: Three views of AE activity located around deposition holes DA3545G01. (Top: Oblique view looking North; Middle: Transverse view looking north; Bottom: Plan view). The different raypaths used in the analysis are also shown.	39
Figure 3-13: Waveforms from selected events shown in relation to a transverse view of AE activity.	40
Figure 3-14: Close up plan view of A) Cluster A containing 54 events; B) Cluster B containing 17 events The background grid is 0.1m in size.	41
Figure 3-15: Temporal response plot of located AEs in the identified clusters for a) Cluster A; b) Cluster B. The plots show number per day on left axes and cumulative number right hand axes.	42
Figure 3-16: Plan view of AEs located around deposition hole DA3545G01 during (a) the excavation phase, (b) monitoring during heating to 31/03/2006, (c) the previous six-month monitoring period, from 01/04/2006 to 30/09/2006 and (d) this reporting period (01/10/2006- 31/03/2007). The red arrows mark the orientation of the principle stress.	43
Figure 4-1: P- and S-wave (a) velocity change and (b) amplitude change from the start of monitoring, plotted alongside temperature (TR6045) and pressure (PB616) measurements in deposition hole DA3545G01. The vertical blue lines differentiate between periods of similar environmental conditions (see Table 4-1).	51
Figure 4-2: Average P- and S-wave velocity change for raypaths on category ‘S1’ together with temperature (TR6045) and total pressure (PB616) (top), Young’s Modulus and Poison’s Ratio change (middle), and Crack Density and Saturation change (bottom).	52
Figure 4-3: Average P- and S-wave velocity change for raypaths on category ‘S3’ together with temperature (TR6045) and total pressure (PB616) (top), Young’s Modulus and Poison’s Ratio change (middle), and Crack Density and Saturation change (bottom).	53
Figure 4-4: Average P- and S-wave velocity change for raypaths on category ‘C1’ together with temperature (TR6045) and total pressure (PB616) (top), Young’s Modulus and Poison’s Ratio change (middle), and Crack Density and Saturation change (bottom).	54
Figure 4-5: Average P- and S-wave velocity change for raypaths on category ‘C2’ together with temperature (TR6045) and total pressure (PB616) (top), Young’s Modulus and Poison’s Ratio change (middle), and Crack Density and Saturation change (bottom).	55

Figure 4-6: Average P- and S-wave velocity change for raypaths on category ‘Far’ together with temperature (TR6045) and total pressure (PB616) (top), Young’s Modulus and Poisson’s Ratio change (middle), and Crack Density and Saturation change (bottom).	56
Figure 4-7: Projections of all AEs located during the heating phase (20 th March 2003 to 31 st March 2007). Events are scaled to location magnitude.	57
Figure 4-8: (a) Number and cumulative number of located events from the start of monitoring, (b) average number of AE events per day (averaged over 17 days) and (c) temperature (TR6045) and pressure (PB616) measurements in deposition hole DA3545G01.	58
Figure 4-9: Schematic diagram of the deposition hole and explanation of changes experienced during Period 1.	59
Figure 4-10: Schematic diagram of the deposition hole and explanation of changes experienced during Period 2.	59
Figure 4-11: Schematic diagram of the deposition hole and explanation of changes experienced during Period 3.	60
Figure 4-12: Schematic diagram of the deposition hole and explanation of changes experienced during Period 4.	60
Figure 4-13: Top: Schematic diagram of the locations of all transducers on a single frame. Left: Photo of a section of the transducer assembly. Right: The transducer assembly during installation.	65
Figure 4-14: Plan view of the array geometry for Deposition Hole DA3545G01 during heating in the Prototype Tunnel. The blue solid lines represent direct raypaths between sondes illustrating their ‘skimming’ nature. The blue dashed line represents a raypath that travels through the deposition hole.	67
Figure 4-15: Schematic diagram of the hardware used for the heating stage in the Prototype Repository. The ultrasonic pulse generator sends a signal to each transmitter and the resulting signal is recorded on each receiver. The receivers are also used to listen for AE activity. The archive PC is required to make a copy of the data for backup purposes.	67
Figure 4-16: Waveforms recorded from one transmitter on the array of sixteen receivers. The gold markers indicate the transmission time. The blue and green markers indicate picked P- and S-wave arrivals respectively.	69
Figure 4-17: Locations of calibration shots obtained from a series of tests at 1 metre intervals down the wall of deposition hole DA3545G01. The two views show that these line up and are located close to the surface of the hole.	72
Figure 4-18: Example waveforms from each of the 16 receiving channels for a ‘pencil-lead break’ test undertaken against the Deposition Hole (DA3545G01) wall 6 metres below the tunnel floor.	72

Table of Tables

Table 3-1: Average number of located AEs per day for six monthly periods between 1 st October 2004 and 31 st March 2007.	35
Table 3-2: Values for the 54 events located in Cluster A.	36
Table 3-3: Values for the 17 events located in Cluster B.	36
Table 3-4: Geomechanical instruments installed on the rock surface within Deposition Hole DA3545G01 or from short boreholes excavated from within the deposition hole, from <i>Goudarzi and Johannesson</i> [2007]. “Height” is the installation position above the concrete floor of the deposition hole. The “Azimuth to Tunnel Axis” is measured counter clockwise to the direction of excavation for the Prototype Tunnel (280° East of North),	37
Table 4-1: Summary of velocity, amplitude and AE variation measured during four periods of temperature and/or pressure change.	48
Table 4-2: Summary of key interpretation of rock response from the ultrasonic measurements.	49
Table 4-3: Summary of ultrasonic monitoring at the Prototype Repository to-date. Response Periods are defined in <i>Haycox et al.</i> [2006a].	63
Table 4-4: Boreholes used for AE monitoring of deposition hole DA3545G01.	66

1 Introduction

This report describes results from acoustic emission (AE) and ultrasonic monitoring around a canister deposition hole (DA3545G01) in the Prototype Repository Experiment at SKB's Hard Rock Laboratory (HRL), Sweden. The monitoring aims to examine changes in the rock mass caused by an experimental repository environment, in particular due to thermal stresses induced from canister heating and pore pressures induced from tunnel sealing. Monitoring of this volume has previously been performed during excavation [Pettitt *et al.*, 1999], and during stages of canister heating and tunnel pressurisation [Haycox *et al.*, 2005a,b; Haycox *et al.*, 2006a,b]. Further information on this monitoring can be found in Appendix I. This report relates to the period between 1st October 2006 and 31st March 2007, and is the fourth of a 6-monthly processing and interpretation of the results for the experiment.

The Prototype Repository Experiment (Figure 1-1) has been designed to simulate a disposal tunnel in a real deep repository for disposal of high-level radioactive waste. Its objective is 'to test and demonstrate the integrated function of the repository components under realistic conditions on a full scale and to compare results with models and assumptions'. The experiment consists of a 90m long, 5m diameter sub-horizontal tunnel excavated in a dioritic granite using a Tunnel Boring Machine (TBM). The rock mass has two main discontinuous sets of sparse, en-echelon fractures [Patel *et al.*, 1997]. The Prototype Repository design incorporates six full-scale canister deposition holes which have been excavated vertically into the floor of the tunnel using a TBM converted to vertical boring. Each deposition hole measures 1.75m in diameter and approximately 8.8m in length. Simulated waste canisters, encased in a bentonite buffer, have been placed into each deposition hole and heated from within by specially designed electric heaters to simulate disposed radioactive material at elevated temperatures. The tunnel was then backfilled using a mixture of bentonite and crushed rock, and sealed using concrete plugs. A range of measurements are made in and around the tunnel and deposition holes.

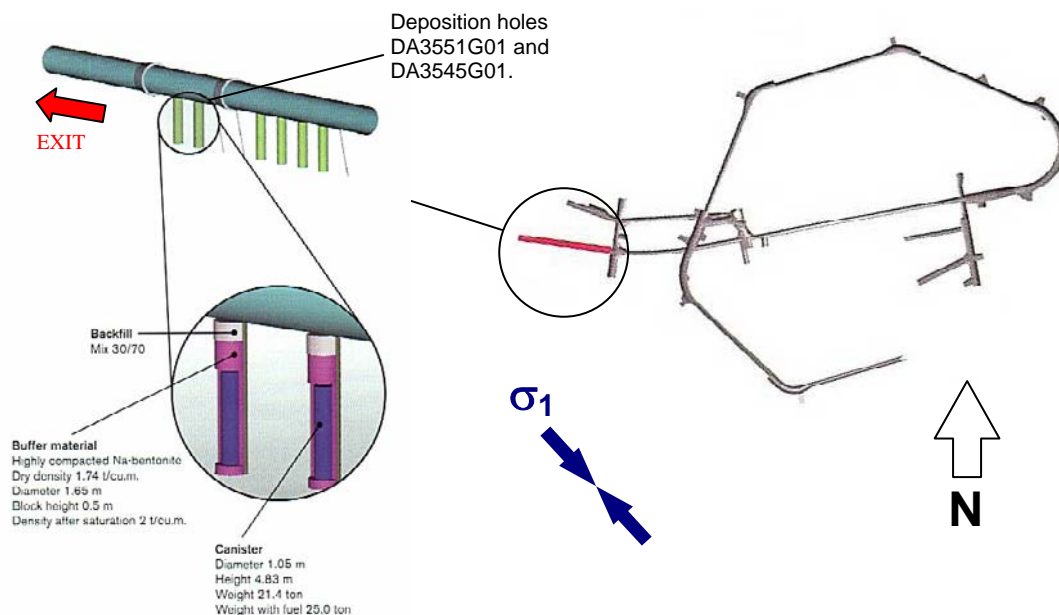


Figure 1-1: Plan view of the experimental tunnels at the Äspö HRL and the location of the Prototype Repository. A schematic illustration of the final experimental set up is shown with canisters and bentonite clay buffer installed in the 1.75m diameter deposition holes. Note the entrance of the tunnel is towards the left. Graphics are modified from SKB[1999].

AE and ultrasonic monitoring is a tool for remotely examining the extent and severity of damage and disturbance around an excavation. This can be induced by the excavation method itself; by the redistribution of stresses (loading or unloading) resulting from the void or by environmental effects such as heating, saturation or pressurisation. Acoustic techniques are particularly adept at assessing the Excavation Damaged or Disturbed Zone (EDZ) as they allow it to be mapped spatially and temporally with high resolution, and they allow the effect on the rock mass to be quantifiably measured. Furthermore, acoustic techniques allow investigations to be conducted remotely, without the need for potentially damaging coring. *Young and Pettitt[2000]* give a review of AE and ultrasonic results from a number of experiments conducted in different underground environments.

- AE monitoring is a ‘passive’ technique similar to earthquake monitoring but on a much smaller distance scale (source dimensions of millimetres). AEs occur on fractures in the rock sample when they are created or when they move. The data acquisition system triggers on AEs when they occur and records full-waveform information that can then be used to delineate the amount, time, location and mechanism of fracturing.
- Ultrasonic surveys are used to ‘actively’ examine the rock. In this case an array of transmitters sends signals to an array of receivers. Amplitude and velocity changes on the ray paths can be interpreted in terms of changes in the material properties of the rock. Calculations using the velocities can determine changes in dynamic moduli, Young’s modulus and Poisson’s ratio, to give direct indications of the properties of the rock through which the raypaths travel. Crack density and saturation can also be calculated to determine changes in crack properties in the damaged and disturbed zones.

Appendix II provides detailed descriptions of the data acquisition and processing used during this, and past, monitoring periods. The ultrasonic array consists of twenty-four ultrasonic transducers configured as eight transmitters and sixteen receivers installed into four instrumentation boreholes using specially designed installation frames sealed within slightly expansive grout. The array is designed to provide good coverage for AE locations and provide ‘skimming’ ray paths so as to sample the rock immediately adjacent to the deposition hole wall. ASC’s InSite Seismic Processor [*Pettitt et al.*, 2005], has been used to automatically process both the AE and ultrasonic survey data. Appendix III A and Appendix III B give the processing parameters used. Data from daily ultrasonic surveys has been automatically picked and arrivals cross-correlated to a reference survey for high-precision measurements of P- and S-wave velocity changes through the experiment. Arrivals of AEs have been manually picked and three dimensional source locations have been calculated.

2 Specific Objectives

This six-month period of ultrasonic monitoring in the Prototype Repository Experiment, has been undertaken with the following objectives:

- Produce accurate source locations for AEs so as to delineate the spatial and temporal extent of any brittle microcracking within the rock mass around the deposition hole and locate any movements on pre-existing macroscopic fractures.
- Conduct regular ultrasonic surveys to assess the effect of heating and other environmental changes on the velocity and amplitude of transmitted ultrasonic waves.
- Investigate changes in dynamic moduli and crack density to show how the properties of the rock volume around the deposition hole change through the experiment.
- Relate the AE and ultrasonic measurements to the measured *in situ* stress regime and other operating parameters such as temperature and fluid pressure.
- Outline how the results from this reporting period relate to previous monitoring periods, and into the overall experimental aims and objectives.

3 Results

3.1 Ultrasonic surveys

An indication of major environmental changes occurring in the tunnel and deposition holes can be ascertained from the temperature and pressure measurements. The temperature in the rock around the deposition hole is shown in Figure 3-1. The temperature on these instruments remains very stable over the six month monitoring period varying by only 0.1 - 0.2 °C.

Figure 3-2a shows total pressure in the tunnel backfill above the deposition hole. Overall, a slow rate of increase (0.05 - 0.08 MPa) is observed in pressure by the instruments in the backfill above the deposition hole. After the 20th February, there is a small decrease in pressure, 0.02 MPa, observed on all the instruments. A constant increase of the pressure in the deposition hole is displayed in Figure 3-2b.

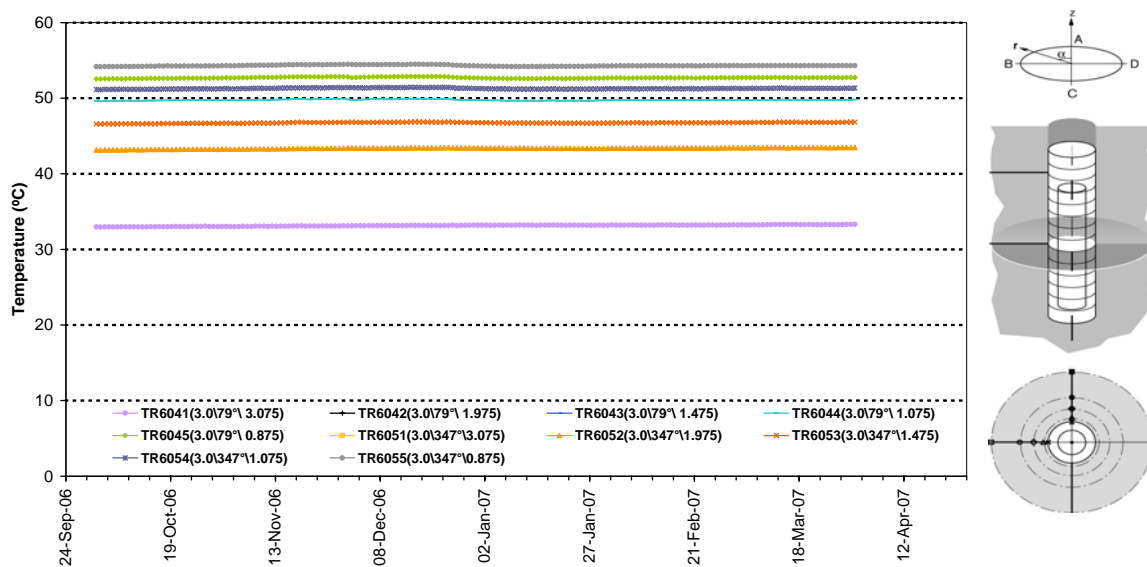


Figure 3-1: Temperature around deposition hole DA3545G01. The sensors are positioned mid-way up the deposition hole with different depths into the rock mass (see right-hand inset) [Goudarzi, 2007].

Velocity changes are measured between transmitter-receiver pairs on the daily ultrasonic surveys using a cross-correlation technique that allows a velocity resolution of $\pm 2 \text{ m.s}^{-1}$. The reference survey for processing ultrasonic results for the previous monitoring periods, with manual P- and S-wave arrival picks, is recorded on 8th December 2004 [Haycox *et al.*, 2006a]. Processing of data recorded during this monitoring period has used the same reference survey so that results can be accurately related to previous periods. Knowing the transmitter and receiver locations, the ultrasonic velocity for each raypath was calculated with an estimated uncertainty

of $\pm 30 \text{ m.s}^{-1}$ (± 3 data points). A cross-correlation procedure was then used to automatically process subsequent surveys. This technique cross-correlates P- and S-wave arrivals from a transmitter-receiver pair with arrivals recorded on the same transmitter-receiver pair on the reference survey. This results in high-precision measurements of P- and S-wave velocity change, with estimated uncertainties of $\pm 2 \text{ m.s}^{-1}$ between surveys. The main reason for the reduction of uncertainty when using the cross-correlation procedure is the dependency of manual picking on the user's judgement of the point of arrival. This can usually be quite indiscriminate because of random noise superimposed on the first few data points of the first break. The cross-correlation procedure then allows for a high-resolution analysis to be performed and hence small changes in velocity to be observed. This is extremely important when changes in rock properties occur over only a small section (5%) of the ray path.

Average P- and S-wave velocity change is shown in Figure 3-3a. We observed a rapid but minor decrease in velocity between the 18th and 20th October 2006. P-wave velocity decreases by $\cong 1.0 \text{ m.s}^{-1}$ and S-wave velocity decreases by $\cong 0.3 \text{ m.s}^{-1}$. Similar changes in velocity over one day have been noted in previous monitoring periods [Haycox *et al.*, 2005b; Haycox *et al.*, 2006a,b]. Following this event, the velocity slightly increases until the start of January 2007. Another rapid but minor increase in P-wave velocity is noted between the 25th and 26th January, 2007 (0.08 m.s^{-1}). The corresponding S-wave increase is smaller (0.03 m.s^{-1}). The velocity remains virtually constant until 18 March 2007 when P- and S-wave velocities show a decrease over one day (0.25 m.s^{-1} and 0.02 m.s^{-1} respectively). The velocity changes observed are of interest, but the magnitude of the change is less than the velocity resolution of 2 m.s^{-1} estimated for ultrasonic measurements. As shown in Figure 3-3a, the rapid changes in velocity in October and January may be linked to a longer-term increase and decrease in temperature.

Amplitude change for this monitoring period is shown in Figure 3-3b. P-wave and S-wave amplitudes decrease between the 18th and 20th October, but the extent of the decrease is not as great as observed for the velocity. Subsequently, the amplitudes exhibit a relatively constant increase. S-waves increase to a greater extent, ending the monitoring period 0.29 dB greater than at the start. P-waves increase by 0.09 dB over this time.

The changes in amplitude and velocity between the 18th and 20th October 2006 have been investigated by looking at the waveforms. An example of how one waveform changes is presented in Figure 3-4a. A decrease in velocity is represented by a displacement in the waveform to the right. The cross correlation, Figure 3-4b, shows a similar pattern. As in previous monitoring periods, not all raypaths are affected in an identical manner, nor are ray paths purely from one instrumentation borehole to another affected. As such, the change is interpreted as a localised change in the general rock properties rather than a systematic change in the measurement devices used in the project.

A discussion of changes throughout the monitoring of the two deposition holes in section 2 of the Prototype Repository is carried out in Section 4.2.

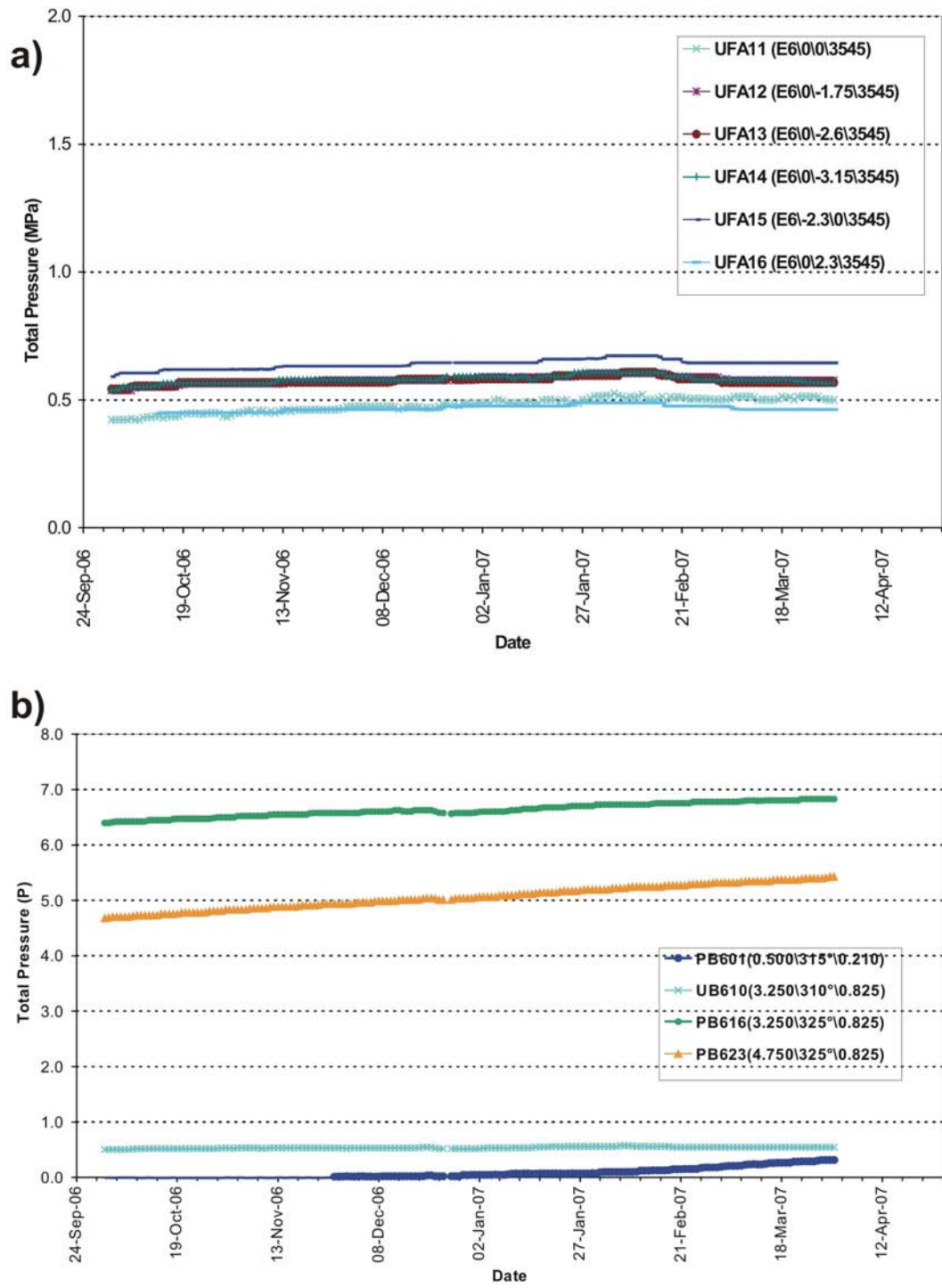


Figure 3-2: Total pressure in (a) the backfill over deposition hole DA3545G01; and (b) in the rock adjacent to deposition hole DA3545G01 [Goudarzi, 2007]. The position of the sensor is presented in the figure legend as distance down, angle around and distance from the axis of the deposition.

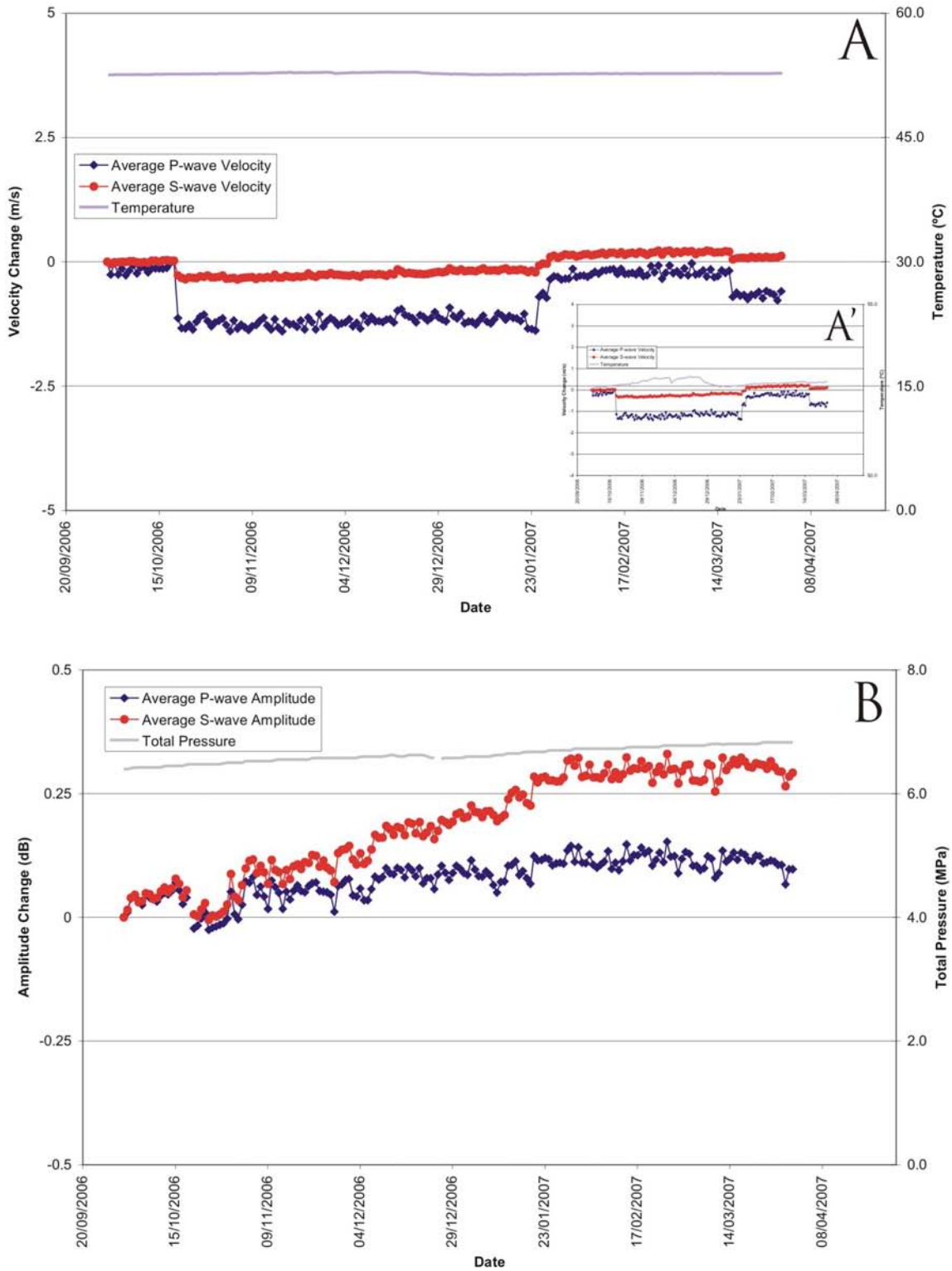


Figure 3-3: Average P- and S- wave (A) velocity change and (B) amplitude change, for the reporting period. Temperature (TR6045) and total pressure (PB616) are displayed on the secondary axes. Chart (A') is a different scale plot of chart (A) just to show changing in temperatures.

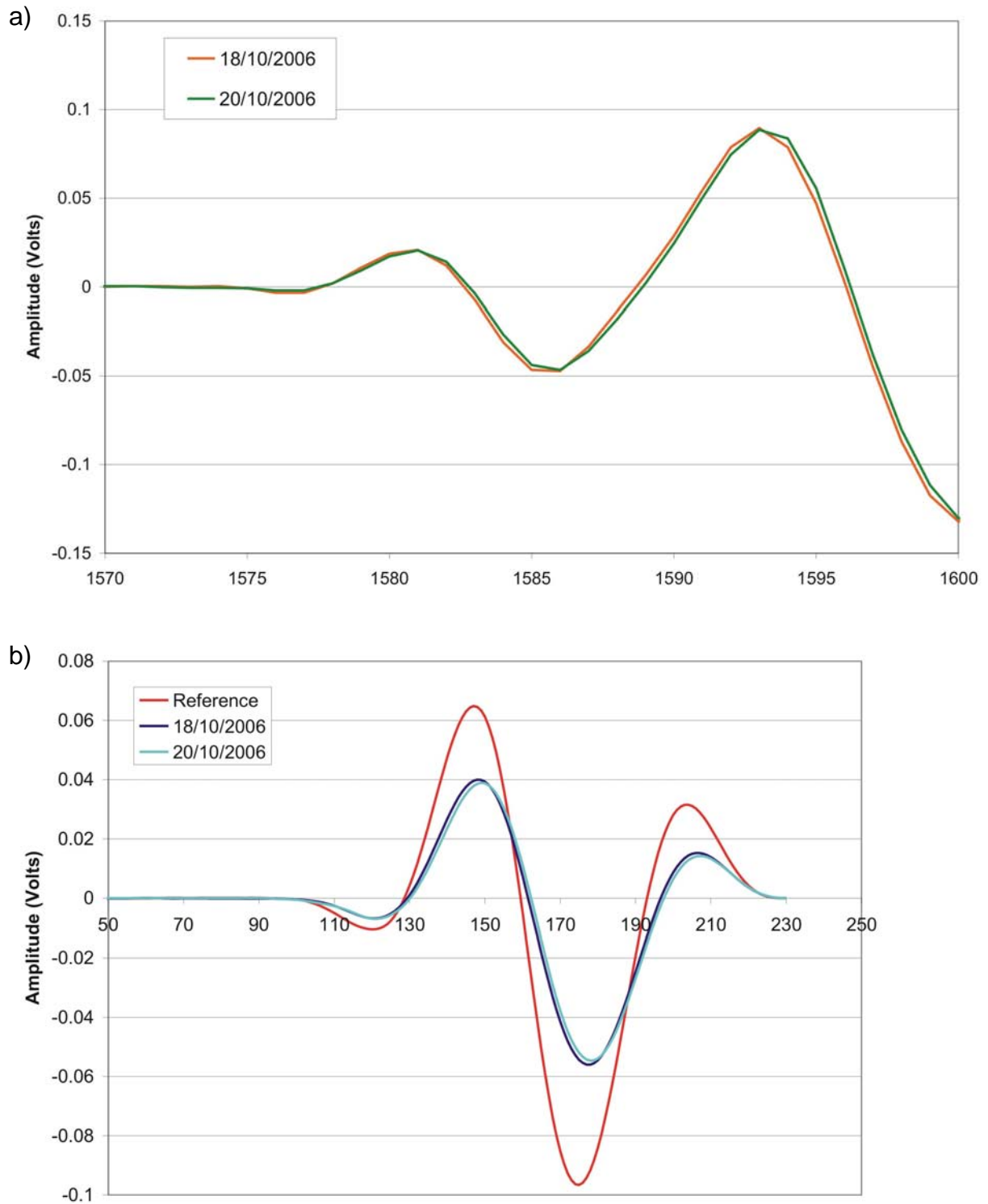


Figure 3-4: Example plots of (a) raw waveform data points and (b) cross correlation windows for the raypath transmitter 5 to receiver 13 on 18th October and 20th October 2007. The second plot shows the reference survey from 8th December 2004.

Pettitt et al.[1999] categorised raypaths from ultrasonic surveys into six types depending on their orientation with respect to the deposition hole and the in situ stress field (Figure 3-5). This figure shows an interpretation of the ultrasonic results in terms of disturbed and damaged regions around the void during the excavation phase of the experiment. *Pettitt et al.*[2000] undertook three-dimensional elastic stress modelling to describe these zones of stress.

Example raypaths from category 'S3' are presented in Figure 3-6. These raypaths pass within centimetres of the deposition hole through the excavation damaged zone, in a region of low compressive or tensile stress. These particular raypaths have been chosen because they provide a comparison of velocity changes down the length of the deposition hole. Each plot of velocity change is accompanied by a schematic diagram giving a perspective of the region through which the raypath passes. For all the four raypaths, very little velocity change is recorded for both P- and S-waves.

Figure 3-7 shows velocity results for raypaths of category 'S1'. These raypaths pass through a region of high compressive stresses and permanent damage close to the deposition hole wall imaged by relatively high AE activity during excavation. During this period, very little change is observed in P- or S-wave velocity.

In order to analyse consistent and small changes in the measurements, Figure 3-8 compares the results of average velocity change across the different raypath categories described in Figure 3-5. P-wave velocities decrease 1.0 m.s^{-1} after the 19th October; a decrease is common for all the raypaths examined. The major decrease, about 1.6 m.s^{-1} , is observed on the C1 raypath. The P-velocity is constant until the 25th January where an increase of 1.0 m.s^{-1} is observed for all the raypaths. A slight decrease in P-velocity ($\cong 0.5 \text{ m.s}^{-1}$ for all the raypaths) occurs on 18th March. S-waves show similar variations but of much lower magnitude (0.1 m.s^{-1} decrease on 19th October, 0.1 m.s^{-1} increase on 25th January and 0.1 m.s^{-1} decrease on 18th March).

Figure 3-9 compares the results of average amplitude change across the different raypath categories given in Figure 3-5. P-wave and S-wave amplitudes decrease on 19th October. After this date, P- and S-waves generally exhibit amplitude increases for the rest of the monitoring period. S-wave amplitudes show more consistent results by raypath, increasing constantly until March. P-wave amplitude results vary more by raypath. The amplitude for category 'C1' does not increase after the initial drop. Similarly, category 'S1' also exhibits little change, ending the monitoring period at virtually the same amplitude as at the start. The biggest amplitude increases are observed in categories 'C2' and 'Far' (0.18 dB and 0.23 dB respectively).

Figure 3-10 shows changes in Young's Modulus, Poisson's Ratio, Crack Density and Saturation Parameters calculated from the average measured velocities for the raypath categories. 'Crack Density' and 'Saturation' of the rock mass are determined using the method of *Zimmerman and King*[1985], as described in Appendix II.

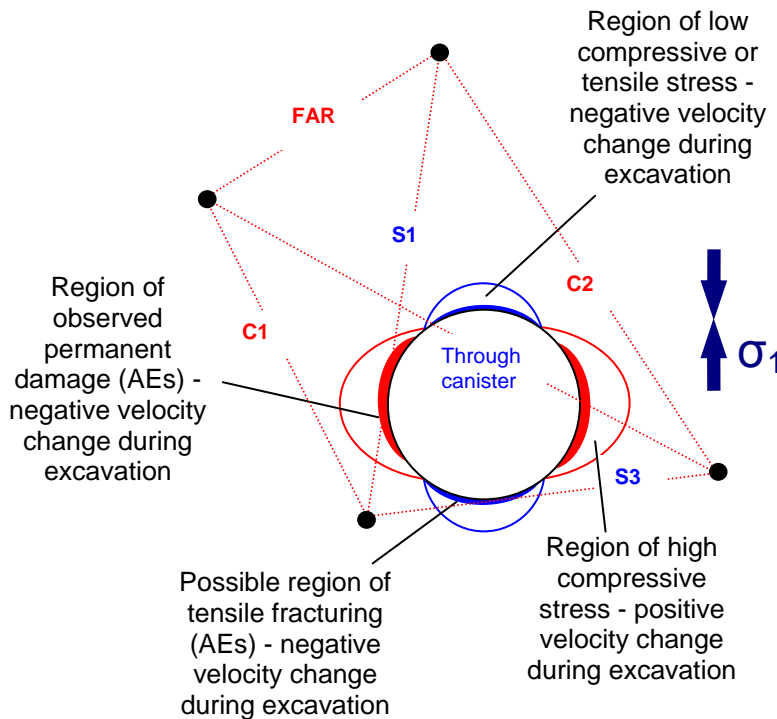


Figure 3-5: Interpretation of the ultrasonic results during excavation in terms of disturbed and damaged regions around the deposition hole. Zones of induced stress are inferred from elastic modelling and the σ_1 orientation. After Pettitt et al.[1999].

Young's Modulus, Poisson's ratio and saturation are observed to decrease on 19th October. The values remain almost constant until the 25th January when an increase is observed. A small decrease occurs again on 18th March. All raypath categories exhibit similar changes during this monitoring period.

Crack density shows the opposite behaviour displaying an increase on 19th October, followed by a decrease on 25th January, and an increase on 18th March 2007. These changes do not coincide with any rapid changes in temperature or pressure, although there is a small-scale change in temperature in the period October-December that may be related. The measured changes are minor adjustments in the rock mass overall leading to a general opening of microcracks in October and March, and general closure of microcracks in January.

During this six month period, the velocity and amplitude results have shown that the rock mass around the deposition hole has not altered significantly. A relatively constant temperature and pressure has led to minor changes in P- and S-wave velocity that are smaller than existing estimated uncertainties. During a relatively stable period of environmental characteristics, no dramatic changes in the rock mass have been measured. This is the result that would be expected during a period of slow pressure increase and little temperature change.

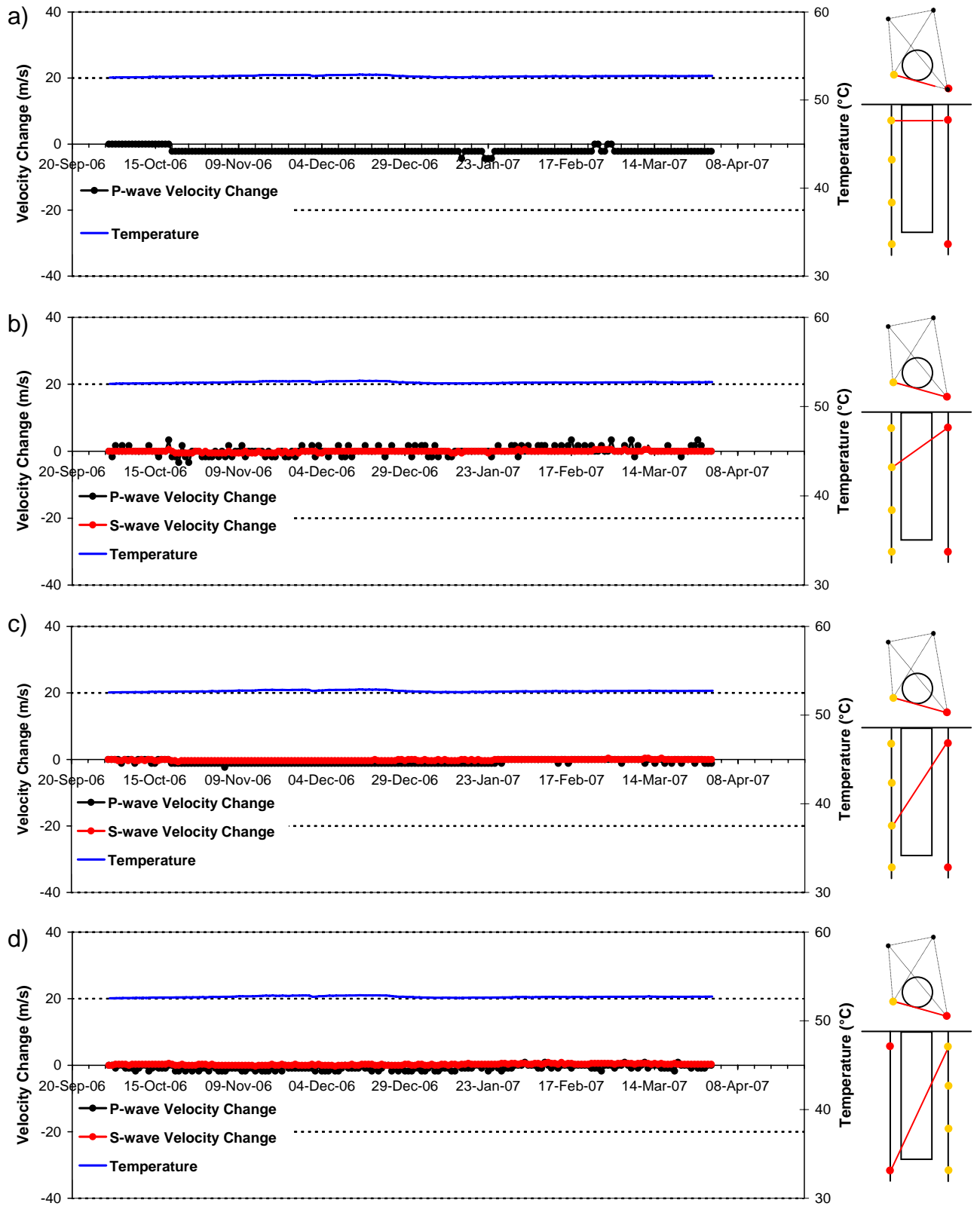


Figure 3-6: Velocity changes measured on ray path category 'S3' (Figure 3-5) for deposition hole DA3545G01. Ray paths shown are from a top transmitter to receivers with increasing depth: a) transmitter, $t_n=1$, receiver, $r_n=5$; b) $t_n=1$, $r_n=6$; c) $t_n=1$, $r_n=7$; d) $t_n=4$, $r_n=1$. Schematic diagrams in the right margin indicate the relative positions of transmitter (red) and receiver (gold). Temperature (TR6045) is displayed on the secondary axes.

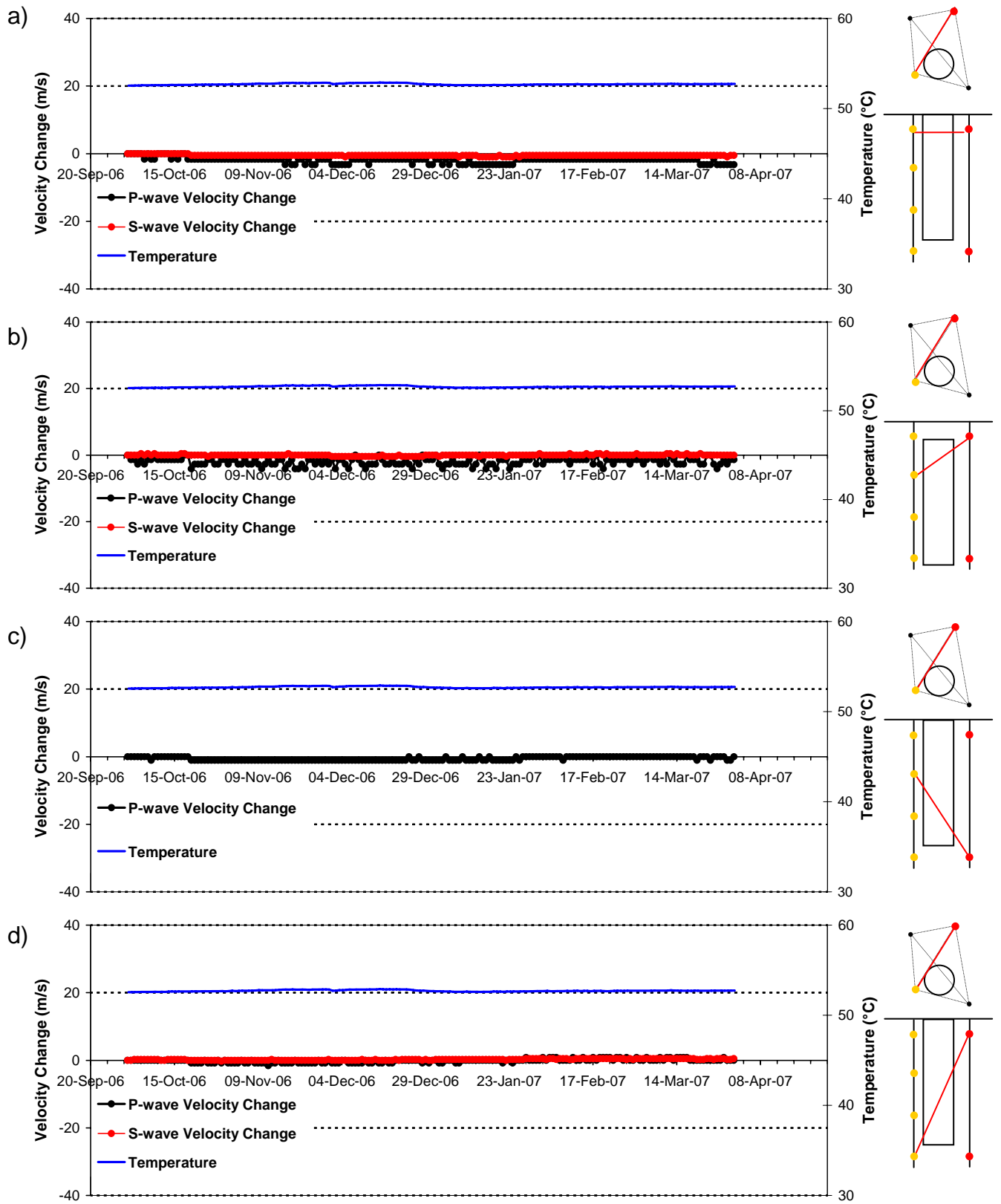


Figure 3-7: Velocity changes measured on ray path category 'S1' (Figure 3-5) for deposition hole DA3545G01. Ray paths shown are from a top transmitter to receivers with increasing depth: a) transmitter, $t_n=7$, receiver, $r_n=5$; b) $t_n=7$, $r_n=6$; c) $t_n=7$, $r_n=7$; d) $t_n=7$, $r_n=8$. Schematic diagrams in the right margin indicate the relative positions of transmitter (red) and receiver (gold). Temperature (TR6045) is displayed on the secondary axes.

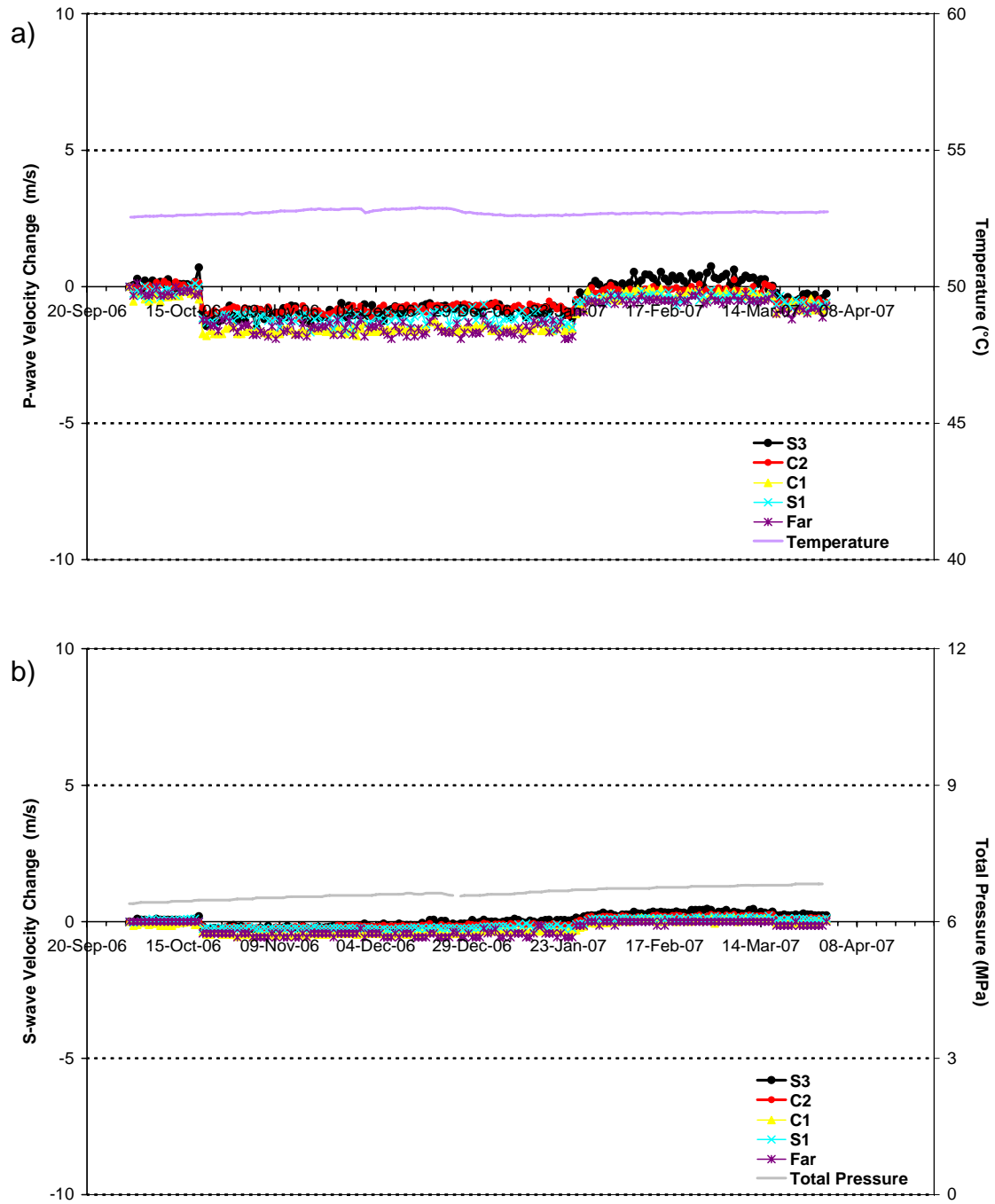


Figure 3-8: Velocity change plots of 5 raypath categories around deposition hole DA3545G01 for (a) P-waves and (b) S-waves. Temperature (TR6045) and total pressure (PB616) are displayed on the secondary axes.

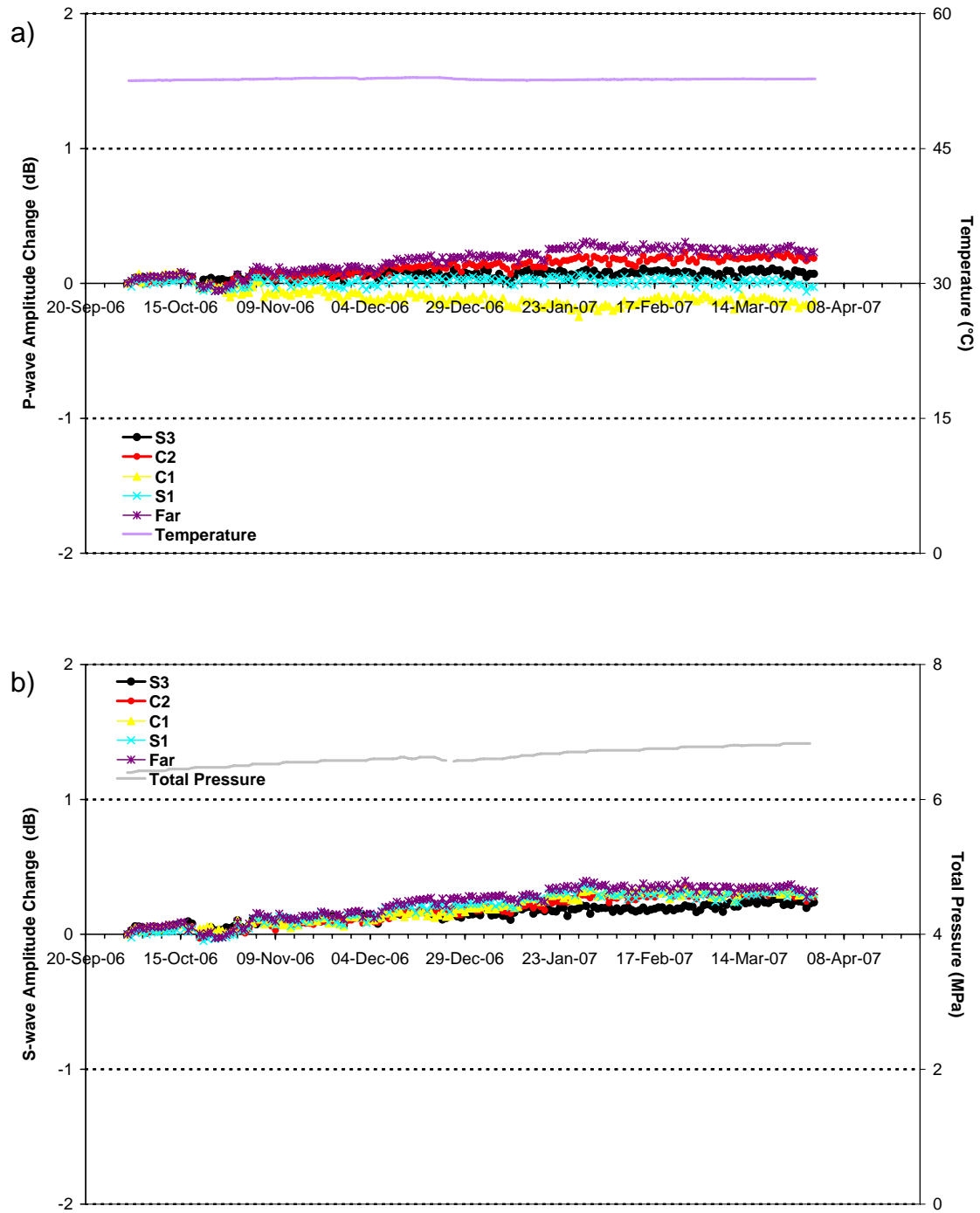


Figure 3-9: Amplitude change plots of 5 raypath categories around deposition hole DA3545G01 for (a) P-waves and (b) S-waves. Temperature (TR6045) and total pressure (PB616) are displayed on the secondary axes.

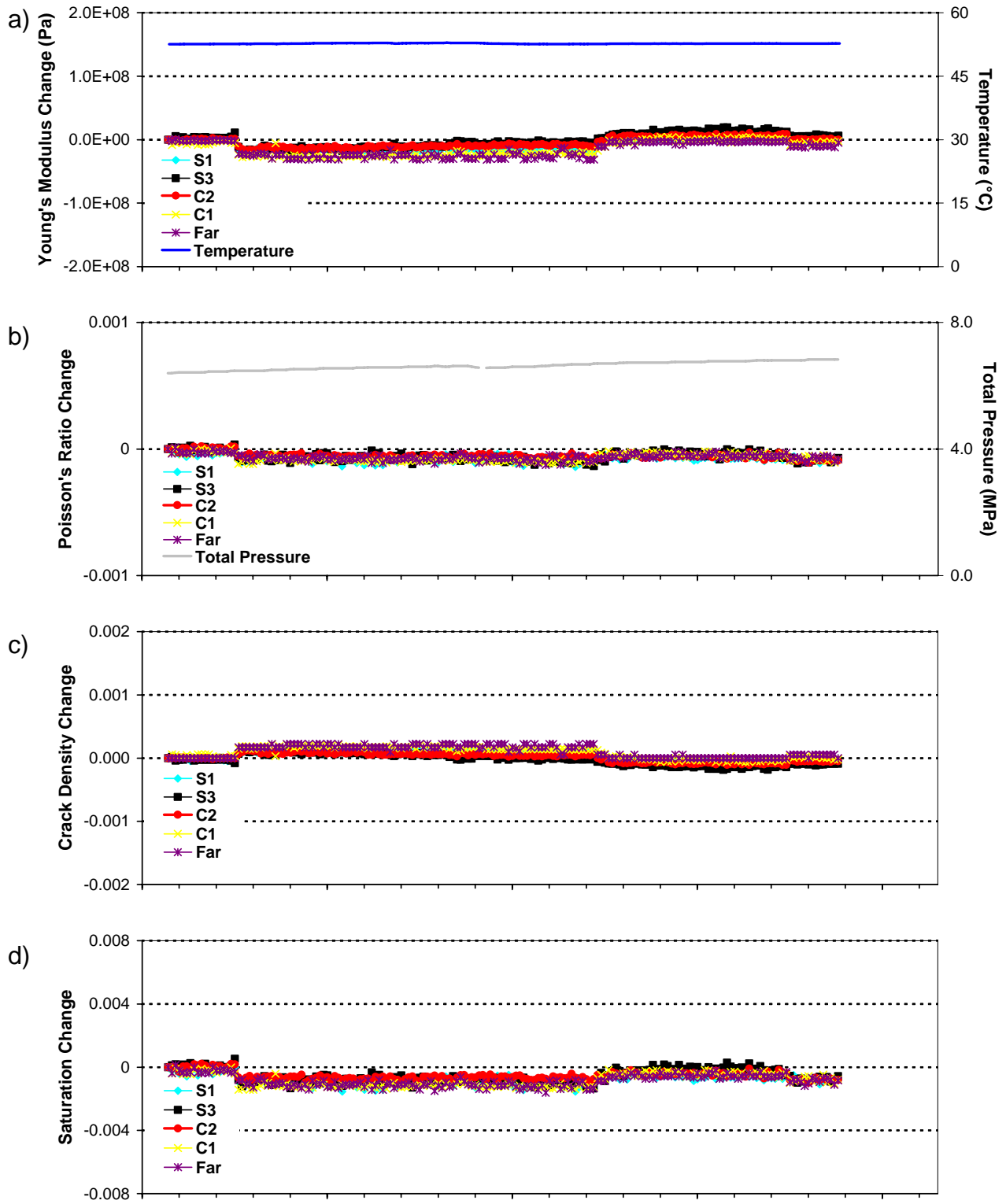


Figure 3-10: Changes in rock parameters during this reporting period for average P - and S -wave velocity values on different raypath orientations. (a) Young's Modulus, (b) Poisson's Ratio, (c) Crack Density and (d) Saturation. Raypath orientations are described in Figure 3-5. Temperature (TR6045) and total pressure (PB616) are displayed on the secondary axes.

3.2 Acoustic Emissions

Processing of AEs has been undertaken following the procedures outlined in Appendix II. 74 events have been located with high confidence from 83 triggered events during this reporting period. The estimated uncertainty for these events is less than 5cm, determined using calibration ‘hits’ performed within the deposition holes after excavation (see Appendix II for further details).

The temporal response of triggers and located events recorded during this monitoring period is shown in Figure 3-11. A trigger is described as an event that has been acquired by the system, but may not be of sufficient energy or quality to be located during the processing procedure. ‘Noise’ events, produced from electrical or man-made sources, have been removed from this count to allow a more accurate representation of fracturing in the rock. The temporal distribution of AE triggers is shown in Figure 3-11a. The temporal response of the 74 located AE events is displayed in Figure 3-11b. A maximum of 3 triggers are recorded on one day, on 30th October 2006 and 2nd February 2007. These dates also relate to the maximum number of located events; three on each day. An average of 0.40 events is located per day during this monitoring period. This represents a decrease from the previous six months, but is greater than the 18 months before that (Table 3-1).

Table 3-1: Average number of located AEs per day for six monthly periods between 1st October 2004 and 31st March 2007.

Time Period	Average Number of Events per Day
1 st October 2004 to 31 st March 2005	0.32
1 st April 2005 to 30 th September 2005	0.21
1 st October 2005 to 31 st March 2006	0.27
1 st April 2006 to 30 th September 2006	0.80
1 st October 2006 to 31 st March 2007	0.40

AEs have been visualised in the InSite Seismic Processor in relation to physical features of the Prototype Repository. Three projections are presented in Figure 3-12 showing the spatial distribution of located AEs. Instrumentation boreholes are represented by brown vertical lines and the tunnel and deposition hole outlines are represented by grey wireframes. The majority of located events locate in two tight clusters at a depth of 455.1m.

As shown in Figure 3-12 two events are located near the tunnel and an isolated shallower event is present near Cluster B. Waveforms of these events are shown in Figure 3-13. This figure shows typical waveforms recorded on different channels and demonstrate the high quality data that is recorded using the array.

Most events (54 AEs) locate in Cluster A on the SE side of deposition hole DA3545G01. This cluster occurs in a position where AEs were observed to locate in previous monitoring periods (Haycox et al., 2006a,b). In the previous six months reporting period, there was no evidence of Cluster B (17 AEs) on the SW of the DA3545G02 deposition hole.

The centre of the events in Cluster A is N,E,D = (268.7, 921.0, 455.1) (Table 3-2). The range of values measured generally supports the accuracy of location measured by calibration hits (see Appendix II). The events are close enough together to be considered occurring on the same feature, as demonstrated by Figure 3-14a which shows a close up plan view of the events. The temporal response of these events is presented in Figure 3-15a. This shows that events in this cluster occur throughout the monitoring period. These AEs occur along the S3 raypath category that passes through a region of low-compressive or tensile stresses.

Cluster B is very tight and the average location of 17 events that compose it is (269.1, 919.7, 455.1) (Table 3-3). This cluster occurs along the S1 raypath that passes through a region characterized by high compressive stresses (Figure 3-5). Figure 3-14b shows a close up plan view of the events. The temporal response of these events is presented in Figure 3-15b.

Table 3-2: Values for the 54 events located in Cluster A.

	Northing (m)	Easting (m)	Depth (m)
Minimum	268.76	921.07	455.11
Maximum	268.83	921.14	455.15
Mean	268.69	920.98	455.06
Standard Deviation	0.018	0.016	0.018

Table 3-3: Values for the 17 events located in Cluster B.

	Northing (m)	Easting (m)	Depth (m)
Minimum	268.96	919.7	455.04
Maximum	269.11	919.82	455.12
Mean	269.07	919.74	455.08
Standard Deviation	0.016	0.016	0.02

Figure 3-16 shows plan views of events recorded during excavation, previous periods of monitoring heating, and this reporting period. The majority of the events are located in the NE and SW quadrants during excavation and initial heating [Pettitt *et al.*, 2000; Pettitt *et al.*, 2002, Haycox *et al.*, 2005a]. These regions are subject to increased compressive stresses, as identified from the insitu stress field by Pettitt *et al.*[1999]. Smaller clusters were observed in the orthogonal regions of low-compressive or tensile stress. It is important to note that events located during this reporting period are consistent with previous results, i.e. no events are positioned in regions where activity has not been observed in the past.

The events are likely to be a continuation of activity in the damage zone, created either by movement on pre-existing microcracks, or as a result of extension or formation of new microcracks in the existing damaged region (see Figure 3-16). A brief study has been conducted to determine whether the event clusters could be caused by movement of one of the many geomechanical instruments placed in the deposition hole for monitoring purposes. This possibility has been discarded given the quoted instrument

positions from *Goudarzi and Johannesson*[2007]. The clusters are both at an average depth of 455.1m, which is approximately 2.0m above the concrete floor of the deposition hole, and at respectively 140°EofN and 240°EofN from the deposition hole axis. Instrument positions are provided in Table 3-4. No instruments are positioned at the correct height, or orientation with respect to the deposition hole axis.

Low magnitudes characterize the entire acoustic emission data set, therefore we can assume that the rock mass around the deposition holes has remained stable during this six-month period. For the past year (this reporting period and *Haycox et al.*[2006b]), a greater proportion of events have been locating in tight clusters in both the low and high compressive regions at a mean depth of 455.1 m. These clusters should be the focus of further investigation.

Table 3-4: Geomechanical instruments installed on the rock surface within Deposition Hole DA3545G01 or from short boreholes excavated from within the deposition hole, from *Goudarzi and Johannesson*[2007]. “Height” is the installation position above the concrete floor of the deposition hole. The “Azimuth to Tunnel Axis” is measured counter clockwise to the direction of excavation for the Prototype Tunnel (280° East of North),

Instrument Type	Label	Height (m)	Azimuth to Tunnel Axis (α), °	Azimuth East of North, °
Temperature (rock surface)	TB610	0.753	270	10
	TB618	2.753	“	“
	TB626	4.253	“	“
Total Pressure	PB609	1.253	325	315
	PB616	3.253	“	“
	PB623	4.753	“	“
Water Pressure	UB604	1.253	310	330
	UB610	3.253	“	“
	UB612	4.753	“	“
Water Content	WB659	3.10	190	90
	WB660	3.25	“	“
	WB661	3.40	“	“
	WB664	4.10	280	0
	WB665	4.25	“	“
	WB666	4.40	“	“
Temperature (in rock)	TR6011-14	Short vertical borehole in floor	-	-
	TR6021-25	Short horizontal borehole at 6.0m	90	190
	TR6031-35	Short horizontal borehole at 6.0m	360	280
	TR6041-45	Short horizontal borehole at 3.0m	90	190
	TR6051-55	Short horizontal borehole at 3.0m	360	280

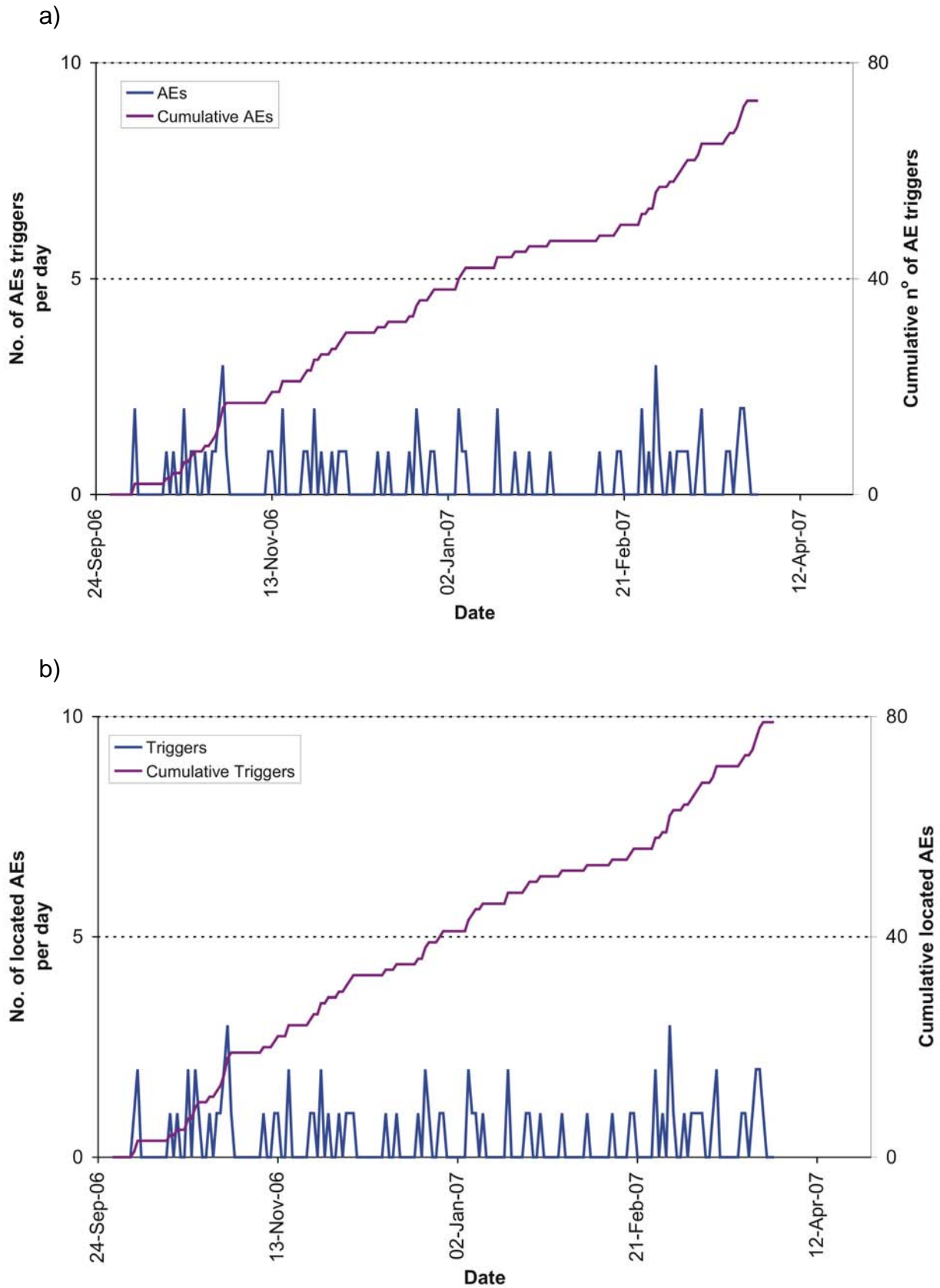


Figure 3-11: Temporal response plot of (a) AE triggers and (b) located AEs; number per day on left axes and cumulative number right hand axes.

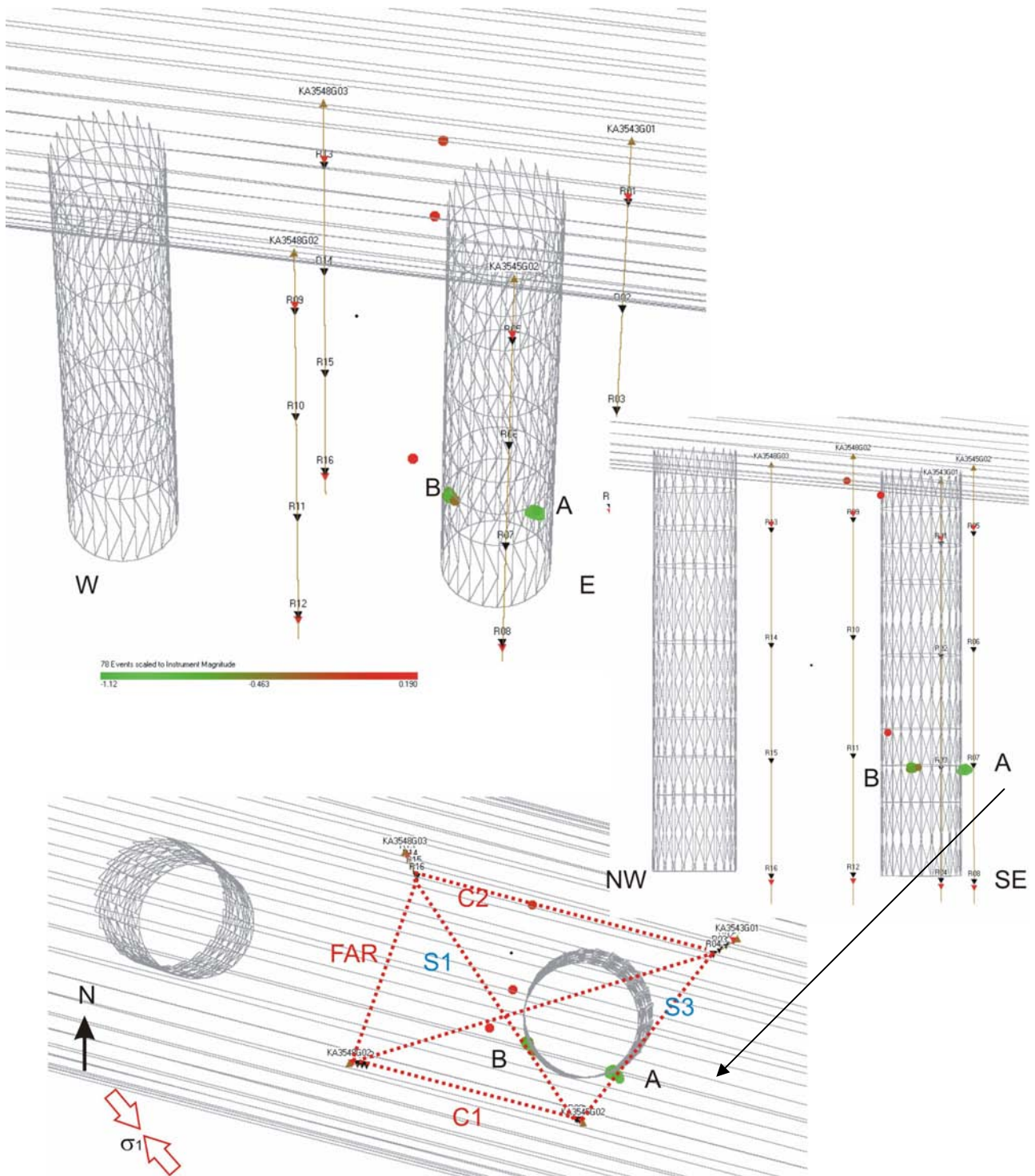


Figure 3-12: Three views of AE activity located around deposition holes DA3545G01. (Top: Oblique view looking North; Middle: Transverse view looking north; Bottom: Plan view). The different raypaths used in the analysis are also shown.

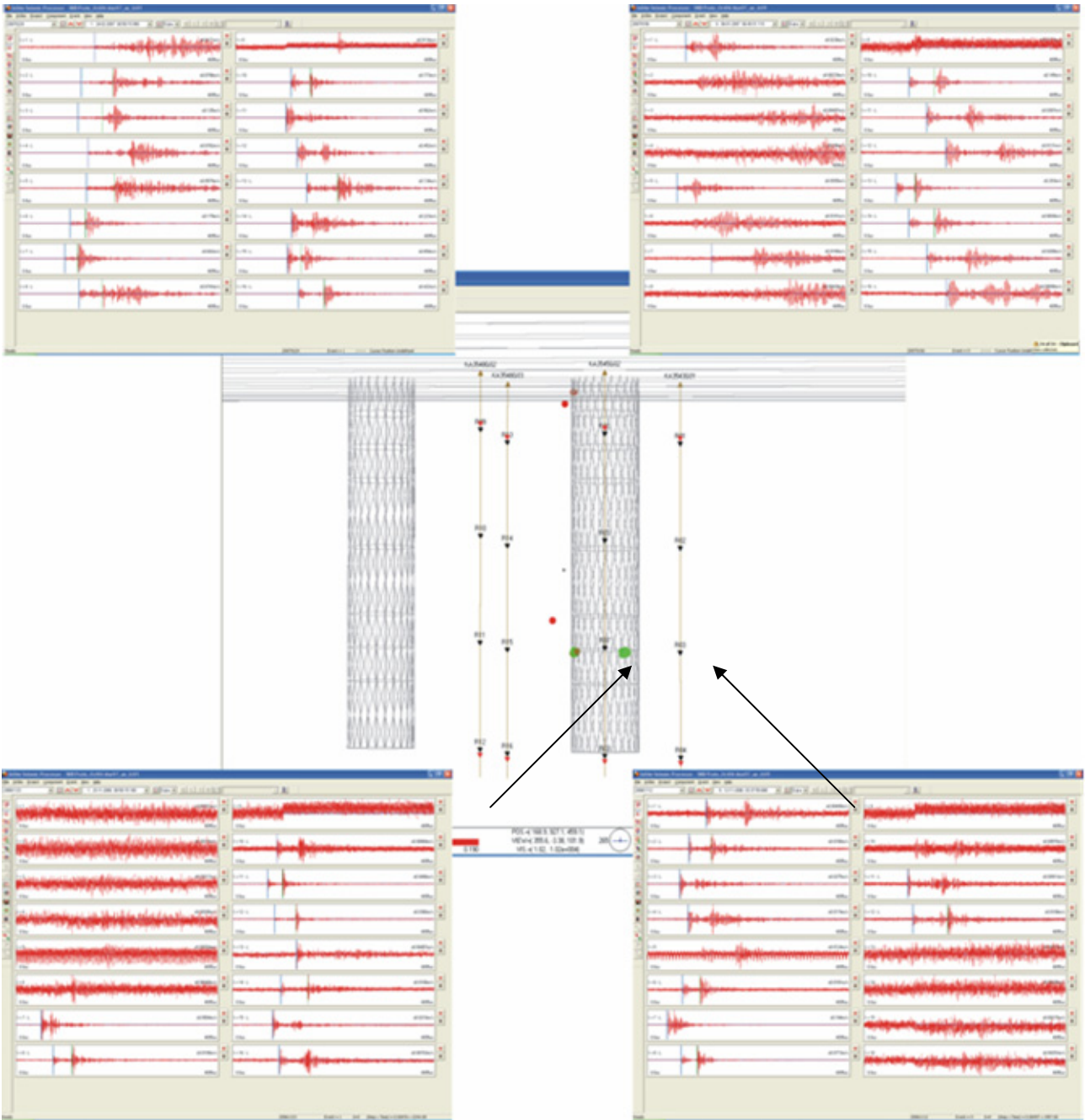


Figure 3-13: Waveforms from selected events shown in relation to a transverse view of AE activity.

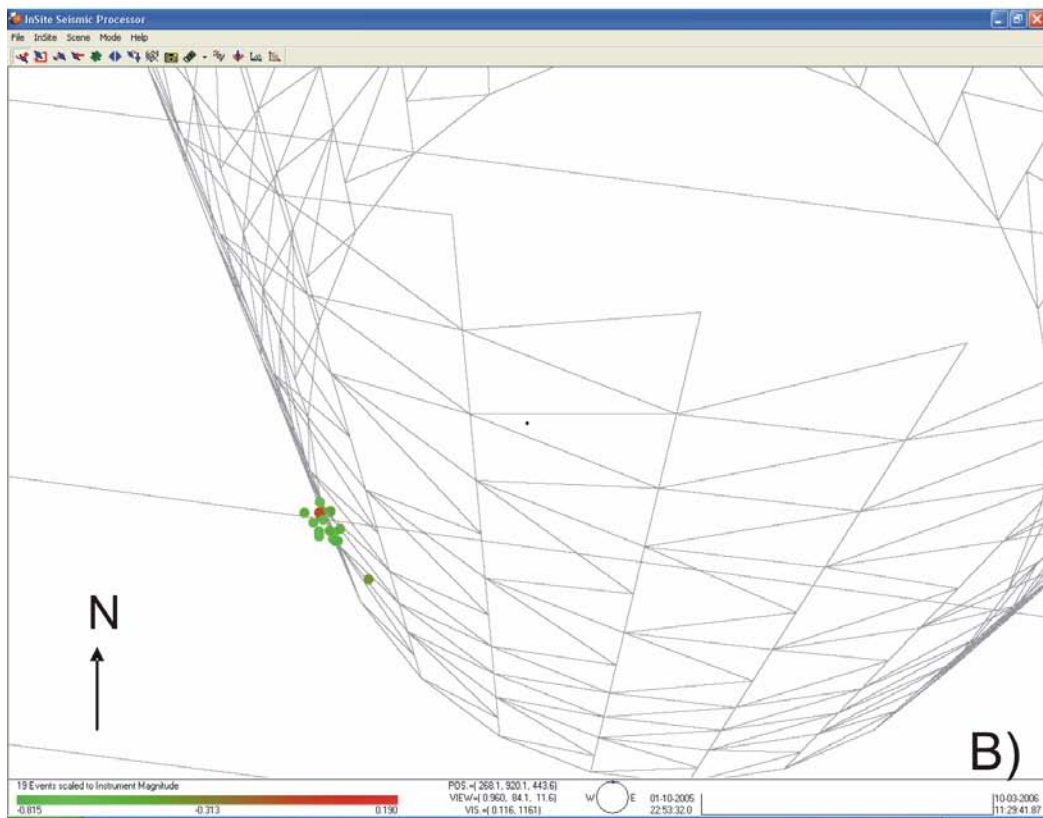
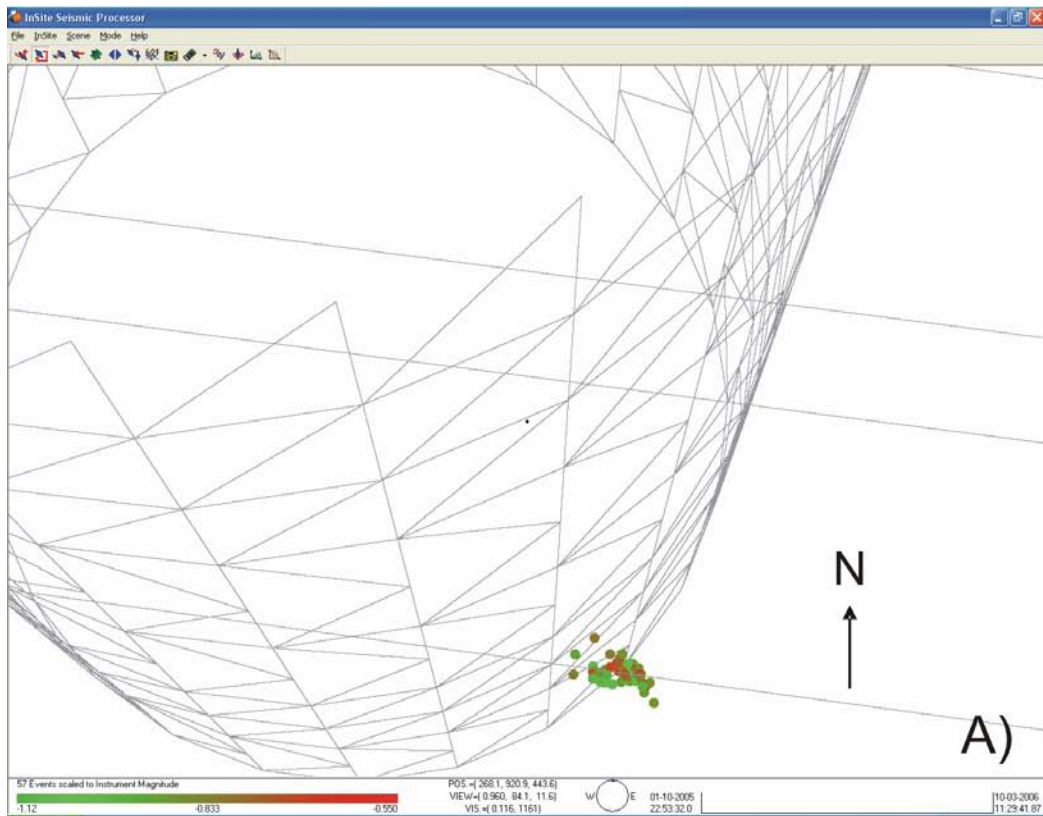


Figure 3-14: Close up plan view of A) Cluster A containing 54 events; B) Cluster B containing 17 events. The background grid is 0.1m in size.

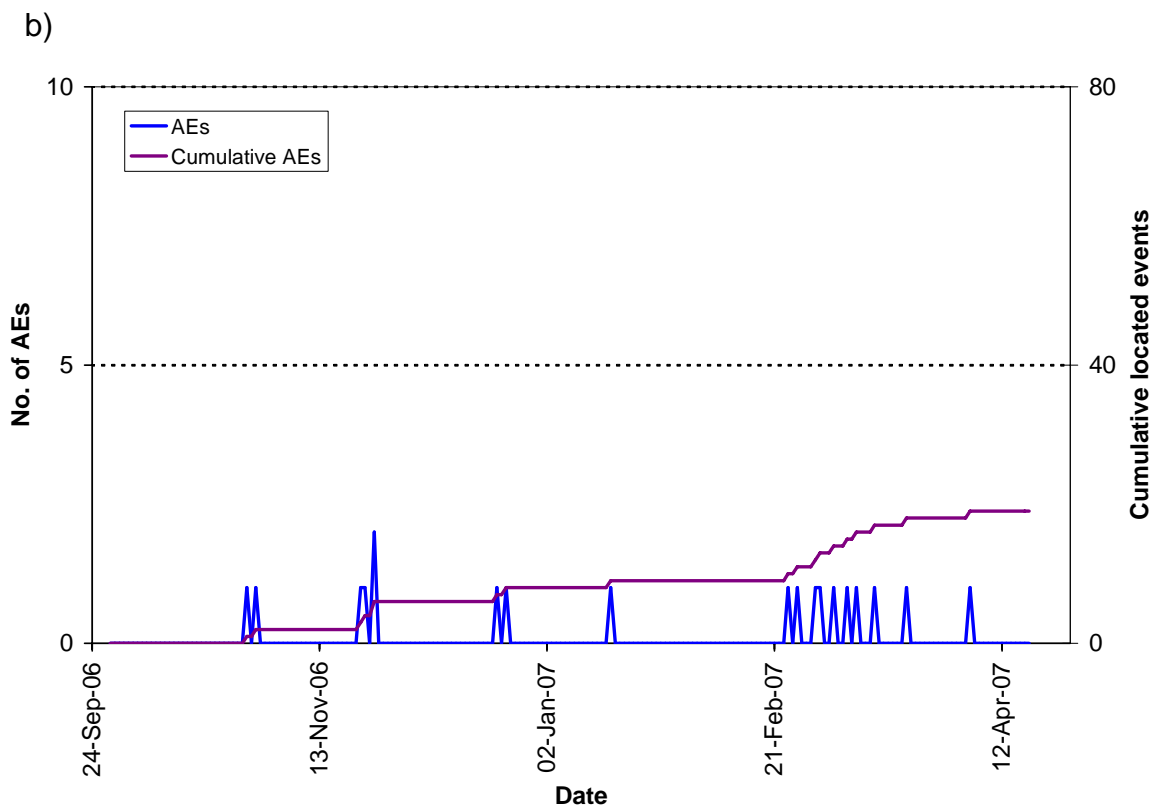
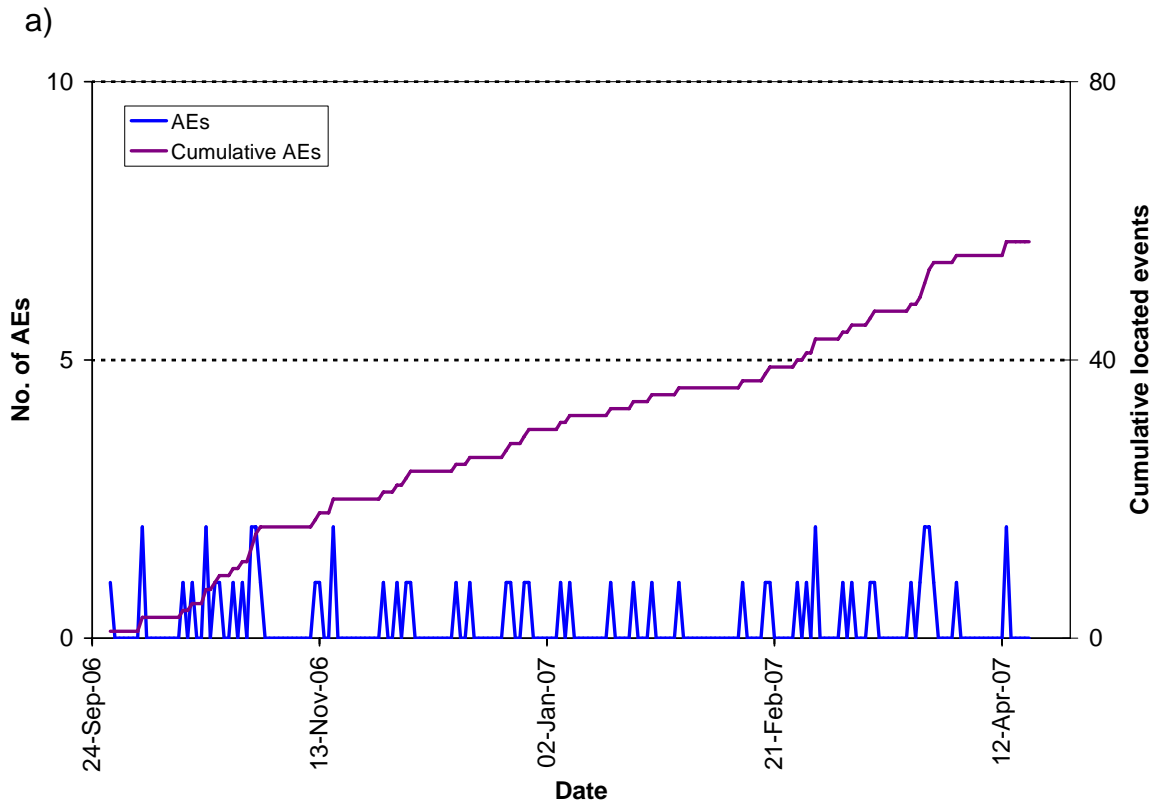


Figure 3-15: Temporal response plot of located AEs in the identified clusters for a) Cluster A; b) Cluster B. The plots show number per day on left axes and cumulative number right hand axes.

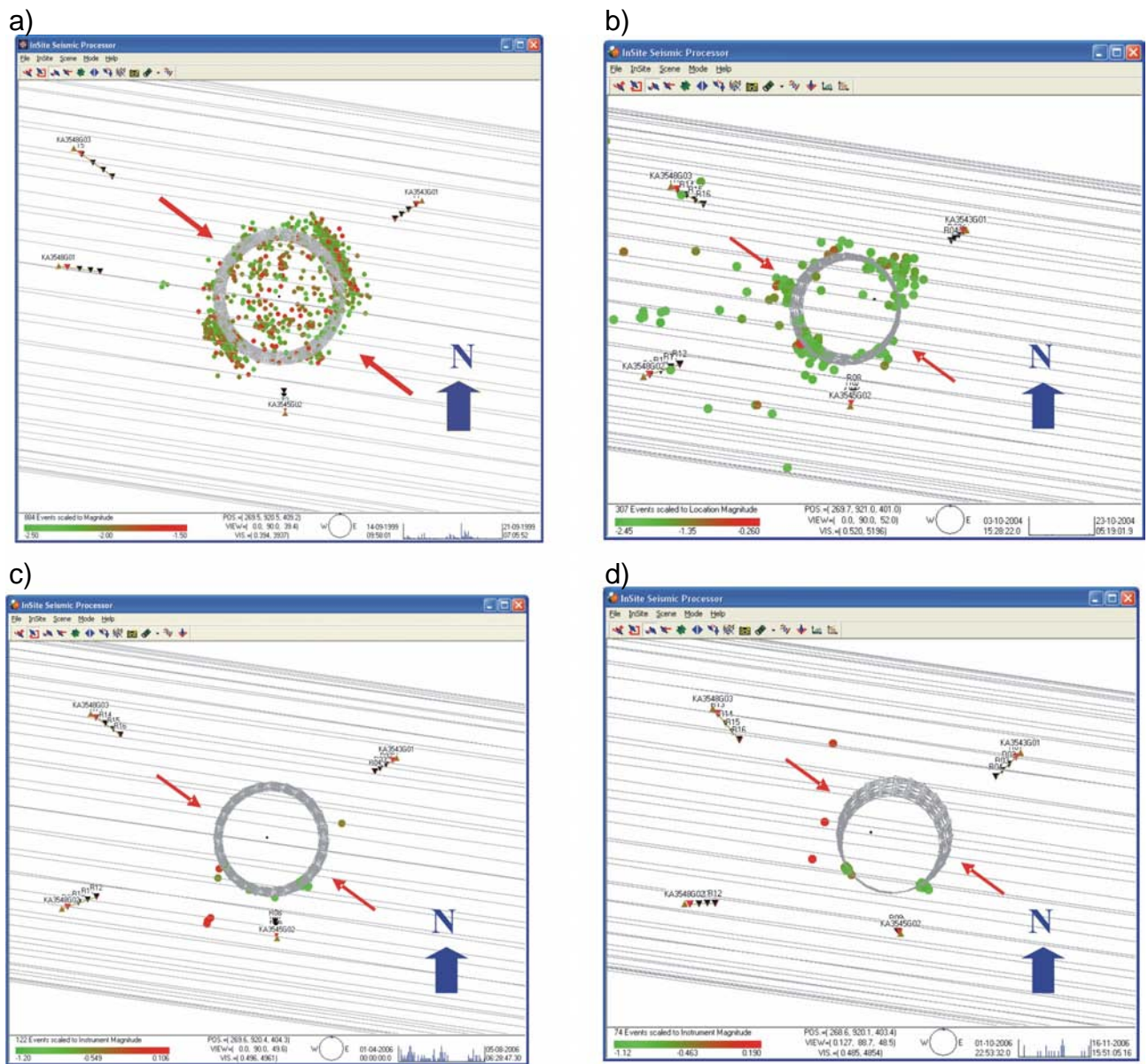


Figure 3-16: Plan view of AEs located around deposition hole DA3545G01 during (a) the excavation phase, (b) monitoring during heating to 31/03/2006, (c) the previous six-month monitoring period, from 01/04/2006 to 30/09/2006 and (d) this reporting period (01/10/2006- 31/03/2007). The red arrows mark the orientation of the principle stress.

4 Conclusions

4.1 Monitoring Between October 2006 and March 2007

- This report describes results from acoustic emission (AE) and ultrasonic monitoring around a canister deposition hole (DA3545G01) in the Prototype Repository Experiment at SKB's Hard Rock Laboratory (HRL), Sweden. The monitoring aims to examine changes in the rock mass caused by an experimental repository environment, in particular due to thermal stresses induced from canister heating and pore pressures induced from tunnel sealing. Monitoring of this volume has previously been performed during excavation [Pettitt *et al.*, 1999], and during stages of canister heating and tunnel pressurisation [Haycox *et al.*, 2005a,b; Haycox *et al.*, 2006a,b]. This report relates to the period between 1st October 2006 and 31st March 2007, and is the fourth of an ongoing 6-monthly processing and interpretation of the results for the experiment.
- The ultrasonic velocity for each raypath is calculated initially on a 'reference survey' with an estimated uncertainty of $\pm 30 \text{ m.s}^{-1}$ (± 3 data points). Velocity changes are measured between transmitter-receiver pairs on the daily ultrasonic surveys using a cross-correlation technique that allows a velocity resolution of $\pm 2 \text{ m.s}^{-1}$. The main reason for the reduction of uncertainty when using the cross-correlation procedure is the dependency of manual picking on the user's judgement of the point of arrival. The cross-correlation procedure then allows for a high-resolution analysis to be performed and hence small changes in velocity to be observed.
- A minor but rapid decrease in velocity occurs between the 18th and 20th October 2006. P-wave velocity decreases by $\cong 1.0 \text{ m.s}^{-1}$ and S-wave velocity decreases by $\cong 0.3 \text{ m.s}^{-1}$. The velocity then exhibits very small increases until the start of January 2007. Another minor but rapid increase in P velocity is noted between the 25th and 26th January, 2007 (0.08 m.s^{-1}). The corresponding S-wave increase is smaller (0.03 m.s^{-1}). The velocity remains virtually constant until 18th March 2007 when P- and S-wave velocities show a decrease over one day (0.25 m.s^{-1} and 0.02 m.s^{-1} respectively). The velocity changes observed are of interest, but the magnitude of the change is less than the velocity resolution of 2 m.s^{-1} estimated for ultrasonic measurements.
- Amplitudes exhibit a relatively constant increase during this monitoring period with S-waves increasing to a greater extent, ending the monitoring period 0.29 dB greater than at the start. P-waves increase by 0.09 dB over this time. Between the 18th and 20th October, P-wave and S-wave amplitude's decrease, but the extent of the decrease is not as great as observed for velocity. After this date, P- and S-waves generally exhibit amplitude increases for the rest of the monitoring period. S-wave amplitudes show more consistent results by raypath, increasing constantly until March. P-wave amplitude results vary more by raypath. The amplitude for category 'C1' does not increase after the initial drop. Similarly, category 'S1' also exhibits little change, ending the monitoring period at virtually the same amplitude as at the start. The biggest amplitude increases are observed in categories 'C2' and 'Far' (0.18 dB and 0.23 dB respectively).

- Changes in Young's Modulus, Poisson's Ratio, Crack Density and Saturation Parameters have been calculated from the average measured velocities for different raypath categories. Young's Modulus, Poisson's ratio and saturation are observed to decrease on 19th October, remain almost constant until the 25th January when an increase is observed, then decrease again on 18th March. All raypath categories exhibit similar changes during this monitoring period. Crack density shows the opposite behaviour displaying an increase on 19th October, followed by a decrease on 25th January, and an increase on 18th March 2007.
- For this reporting period, 74 acoustic emissions have been located with high confidence from 83 triggered events. The rate of triggers remains reasonably constant for all the period, a maximum of three events being located on a single day.
- When the spatial distribution of AEs is studied, 54 of the 74 located events are observed to locate in a very tight cluster at a depth of 455.1 m on the south-east of deposition hole DA3545G01. In the previous six months reporting period 109 were located in this position. The cluster locates in a region of low-compressive or tensile stresses. Another cluster of 17 events locate on the south-west side of deposition hole DA3545G01 at a similar depth to the other cluster. No evidence of this cluster was noted in the previous six months monitoring period. Events in the two clusters are close enough together to be considered as occurring on the same feature and occur over the whole reporting period with no significant peaks in activity. AEs may be occurring at this position due to the presence of a pre-existing microcrack, generated during excavation. A brief study has been conducted to determine whether the event clusters could be caused by movement of one of the many geomechanical instruments placed in the deposition hole for monitoring purposes. This possibility has been discarded as no instruments are positioned at the correct height, or orientation with respect to the deposition hole axis.
- It is important to note that events located during this reporting period are consistent with previous results, i.e. no events are positioned in regions where activity has not been observed in the past. The events can therefore be interpreted as a continuation of activity in the damage zone, and could be created either by movement on pre-existing microcracks, or as a result of extension or formation of new microcracks in the existing damaged region. The numbers of events are relatively low and therefore indicate the rock mass around the deposition holes has remained stable during this six-month period.

4.2 Summary of Monitoring from the Heating and Pressurisation Phase

- Monitoring of the heating and pressurisation phase at the Prototype Repository Experiment has been conducted since March 2003. *Haycox et al.*[2006a] present a detailed analysis of the ultrasonic measurements, and split the experiment into four periods for analysis based on environmental factors (Figure 4-1). Monitoring of the past six months has shown the rock response to be a continuation of the fourth period starting November 2005 consistent with temperature and pressure measurements from other instruments during this reporting period [*Gourdazi, 2007*] that show a slow increase, with no sudden or high magnitude changes. Table 4-1 presents a summary of the observations from ultrasonic monitoring thus far, and Table 4-2 provides interpretations of the rock response after *Haycox et al.*[2006a].
- Figure 4-1 shows average P- and S-wave velocity and amplitude recorded during the monitoring. Figure 4-2 to Figure 4-6 provides average velocity and modulus changes for the six raypath categories selected in terms of disturbed and damaged regions (Figure 3-5). Figure 4-7 and Figure 4-8 show all locations and the temporal distribution of located AEs recorded since March 2006. Figure 4-9 to Figure 4-12 summarise changes that take place at different regions around the deposition hole in schematic diagrams for each period, identifying the primary changes in the properties of the rock as described in Table 4-2.

4.3 Recommendations

The rock mass around the deposition holes has remained stable during the monitoring period and the parameters we investigate show no significant changes, as expected when temperature and pressure remain constant. AE clusters, located with high confidence, occur in a region of pre-existing microcracks and might suggest a re-activation of pre-existing fractures or their association to an instrument located on the deposition hole wall. The acquisition system and instrumentation has been successfully operating at the HRL since 2003. It is recommended that ultrasonic and acoustic emission monitoring is continued, particularly to record during the cooling phase. During cooling, the rock mass may experience changes that can be observed remotely using the ultrasonic tools to monitor the rock.

Clusters of events are observed to locate on the SW and SE walls of the deposition hole. It would be interesting to carry out further study on these events to investigate their mechanisms of failure and how they have changed over time, in relation to changing environmental variables. The objective would be to resolve the primary factors responsible for causing AEs in that particular position.

Table 4-1: Summary of velocity, amplitude and AE variation measured during four periods of temperature and/or pressure change.

Name / Date	Temperature/Pressure	Velocity	Amplitude	AE
PERIOD 1 25 th May 2003 to 31 st October 2004	Heaters in canister switched on causing an initially rapid change in temperature which gradually levels out to a constant increase. An increase of 35°C is measured for an instrument in rock adjacent to the deposition hole. Pressure constant	Rapid increase in P- and S-wave velocity on 'S3' category. Other categories show increases but to a lesser extent. Initial decrease in P-wave velocity in comparison to S-wave velocity for all raypaths except for 'S3'.	Amplitudes increase over this period by between 3dB and 9dB for P-wave amplitude, and 7dB and 12dB for S-wave amplitude.	AEs do not start immediately after heating. This could be a Kaiser-type effect in which AE rate remains close to background level until stress increases above the largest previous value. Peak of 13 events located on 26 th June 2003. Average Event Rate = 0.5 / day
PERIOD 2 1 st November 2004 to 4 th September 2005	Drainage to tunnel closed on 1 st November. Pressure in tunnel increases. Pressure increases measured in the deposition-hole buffer between 3 rd and 5 th December. Damage observed on canister on 6 th December so drainage reopened and heaters switched off. Power switched on 15 th December.	Velocity increases measured close to the tunnel from 26 th November. Larger increases measured on categories 'S1' and 'S3'.	Amplitude increases measured close to the tunnel from 26 th November.	Relatively large number of events recorded in this period. Peak rate of 32 AEs on 4 th and 5 th December. Events locate in clusters in previously observed damage zone. Average Event Rate = 0.4 / day
PERIOD 3 5 th September 2005 to 2 nd November 2005	Additional drainage is opened in August 2005 leading to a decrease in pressure and temperature. Heaters turned off on 5 th September	P- and S-wave velocities decrease on all raypath categories except 'far'.	P-wave amplitude decrease on all category raypaths.	Slight increase in event rate above background rate recorded in previous 5 months. Average Event Rate = 0.3 / day
PERIOD 4 3 rd November 2005 to 31 st March 2007	Pressure in tunnel increases. Constant increase in pressure in buffer above deposition hole. Heaters switched on again so temperature around deposition hole increases.	P- and S-wave velocities increase on all category raypaths. Larger increases measured on 'S3'.	P- and S-wave amplitude increase on the majority of raypaths.	Cluster of 202 events located on SE side of deposition hole. Similar rate of AE locations. Average Event Rate = 0.35 / day

Table 4-2: Summary of key interpretation of rock response from the ultrasonic measurements.

Period	Summary of Key Interpretations
1	<p>The heaters are switched on. The 'S3' category passes through a volume that is unloaded and hence experiences low compressive stresses. This volume responds more rapidly to thermal stresses because existing microfractures are initially unloaded and hence more open than microfractures in the compressive region. P- and S-wave velocities decrease a similar amount during excavation as they increase during heating. This suggests very strongly that the microfractures induced in the regions of tensile damage around the deposition hole close when thermal stresses are applied. The difference in the rate of response between raypaths in the compressive categories was interpreted as a different magnitude of response of the microfractures in the rock mass to increasing thermal stresses.</p> <p>In the first few months of heating, another effect is superimposed onto the rock's response to thermal stresses. This is measured as a reduction in P-wave velocities compared to S-wave velocities in the first few months of heating. This is particularly noticeable on 'S1' category in Figure 4-2, in which P-wave velocity decreases by about $3.5\text{m}\cdot\text{s}^{-1}$ while S-wave velocity remains constant. A desaturation occurs on all raypath categories, other than 'S3'. This must be caused by a drying of the rock mass, in the zones experiencing high compressive stresses, as heat is applied to the rock (i.e. both temperature and pressure are acting to expel moisture). In the low-compressed, or tensile, region saturation increases during this period. This is probably caused by hot fluids expanding into the open microfracture fabric.</p>
2	<p>Pressure rose rapidly after drainage from the tunnel was closed. This resulted in damage to the canister and the heaters being temporarily switched off. Temperature around the deposition hole dropped rapidly, but started increasing again after 13 days. Significant changes to the character of many recorded ultrasonic waveforms were observed as significant increases in signal quality. This suggests that as pressure increased in the rock surrounding the deposition hole, attenuation of the ultrasonic waves is significantly reduced meaning that they can pass more efficiently through the rock medium.</p> <p>The pressure increase can be interpreted as increasing the stiffness of the rock with a corresponding decrease in crack density. The magnitude of increase is greater for 'S1' and 'S3' categories because the volumes through which they pass are close to the deposition holes and contain a higher proportion of microfractures in an excavation damage zone. The pressure increase acts as a confining pressure on the rock mass leading to a closure of the pre-existing microcrack fabric and therefore a reduction in crack density. We observe that only a relatively small pressure increase is sufficient to close this microcrack fabric in the volumes already under high compressive stresses, leading to an initially high rate of change in measured velocities followed by a constant level, even though pressures may keep increasing afterwards. From Figure 4-2 the required pressure increase is approximately 1.5MPa.</p> <p>The rapid pressure increase led to 32 events locating in clusters over the course of two days. The events are interpreted as stress changes in the rock as it responds to the sudden pressure change. This induces small scale movement on pre-existing microcracks, or induces new microfractures in weaker volumes of the rock. Pore pressure increases may also have assisted in inducing slip on pre-existing microfractures, by reducing the normal stress on the fractures. Over the rest of this period, as pressure continued to increase, fewer events were located.</p> <p>Another effect at this time is a rapid cooling of the rock when the heater inside the canister is switched off (for 13 days between 2nd and 15th December 2004), followed by warming as the rock is reheated. The majority of categories do not show a significant change in P- or S-wave velocity during this period indicating they are relatively insensitive to temperature changes at this time (i.e. when pressures are high). The exception is category 'S3', which exhibits a decrease in P- and S-wave velocity followed by an increase that mirrors the rate at which temperature changes (Figure 4-3). This category was found to be the most sensitive to thermal stresses during the initial stages of heating. When the rock cools, thermal stresses acting in this volume of low compressive (or slightly tensile) stresses reduce causing unloading of the microcracks. Microcracks close again when the rock is reheated and thermal stresses increase.</p>

3	<p>In September 2005 additional drainage from a permeable mat placed on the inner surface of the outer plug was opened, and heaters were switched off. This resulted in a cooling and de-pressurisation of the deposition hole. Neither temperature nor pressure reduced to the background level.</p> <p>The decrease in velocity on most raypaths is generally low compared to the increases observed previously. An exception to this is category 'S3'. This category is observed as the most sensitive. As temperature and pressure decreases, stresses again reduce in this volume causing microcracks to reopen and resulting in an increase in crack density and reduced stiffness of the rock.</p> <p>At the start of the period a sudden (over a few days), but relatively small change in velocity is observed, superimposed on the longer-term trends. We believe these are related to rapid changes in fluid pressure; a corresponding increase is observed at the end of the period (start of Period 4). For Period 3, an increase in Young's Modulus occurs which indicates a stiffening of the rock. This short term change is therefore likely to be a sudden reaction of the rock mass to the decrease in fluid pressure, perhaps caused by a general closing of microcracks caused by decreased pore pressures. The reverse is true for Period 4, when a pressure increase leads to a general opening of microcracks caused by increased pore pressures. This is believed to be a different response to long term trends from thermal stresses and general confining of the rock mass.</p>
4	<p>During the fourth period, heaters were turned back on once more causing temperature around the deposition hole to increase. Pressure increased rapidly again, probably caused by changes in the buffer temperature (changes in water volume caused by the temperature in combination with low hydraulic conductivity) [Johannesson, 2006]. Velocity increases rapidly at first, then at a constant rate, following a similar pattern to the temperature and pressure.</p> <p>Raypath category 'S3' exhibits the greatest increase in P and S-wave velocity. Similar patterns are observed on 'S1' and 'C1', and to a lesser extent on 'C2'. Velocity on the 'far' raypath category remains constant throughout the period. When temperature and pressure start to increase the stiffness of the rock increases, particularly on 'S3'. This is accompanied by a reduction in crack density. The associated increase in stiffness and decrease in crack density can be interpreted as the closing of existing microfractures and pore spaces as observed previously. This effect has continued to the current day.</p> <p>Few events have been located during Periods 3 and 4. A rapid decrease, and then increase, in pressure and temperature appears to have no significant affect on the number, or distribution of AEs around the deposition hole. The AE rate has been marginally increasing since February 2006 (Figure 4-8). The vast majority of events locate on a single cluster in the south-east of the deposition hole and at 455.1m depth. Additional events have also been observed in a cluster on the south-west of the deposition hole at a similar depth. The low number of AEs suggests the rock mass has stabilised. The high pressures result in a confining pressure being placed on the rock around the deposition hole and inhibit the movement on microcracks or macrofractures.</p>

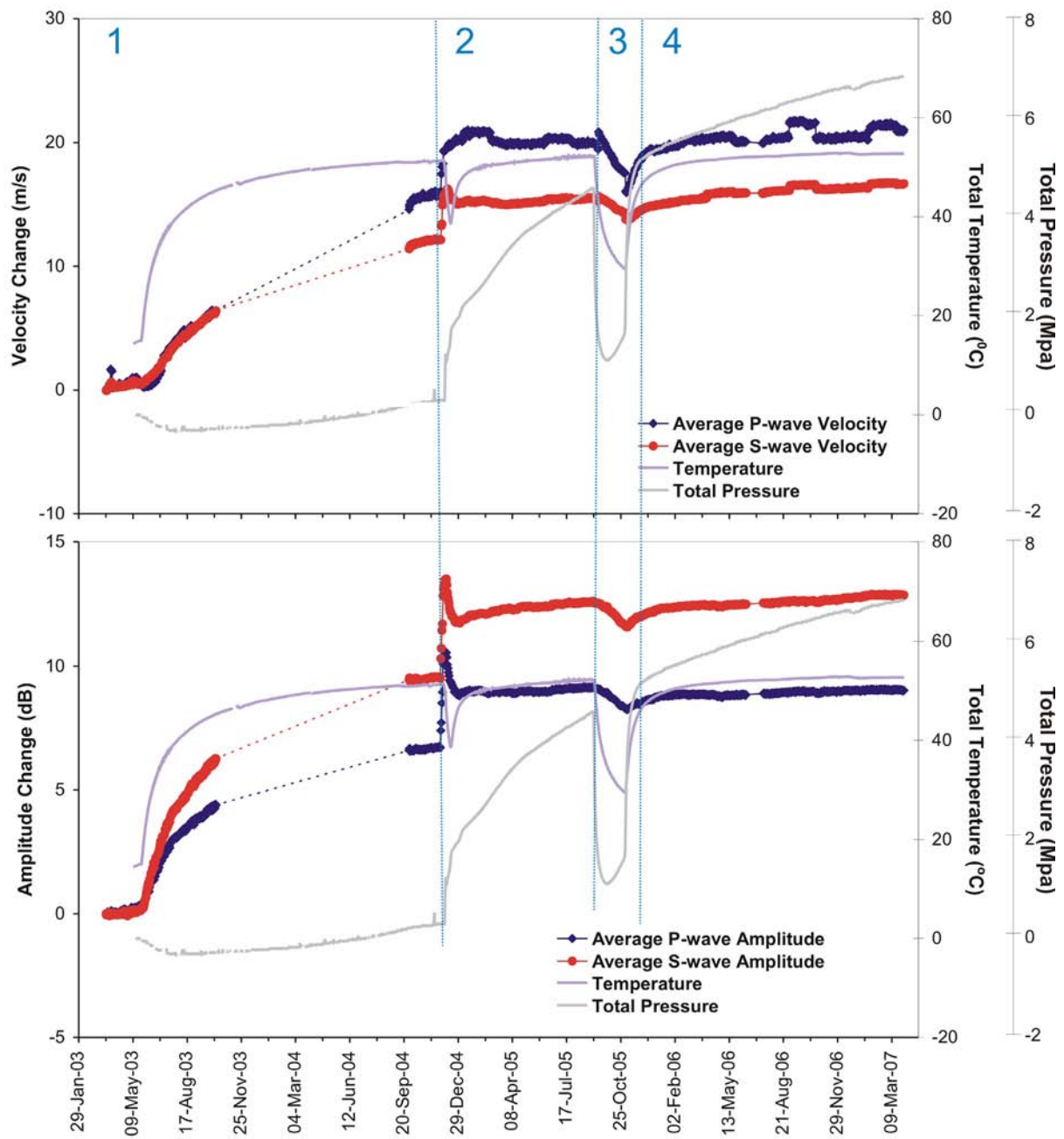


Figure 4-1: P- and S-wave (a) velocity change and (b) amplitude change from the start of monitoring, plotted alongside temperature (TR6045) and pressure (PB616) measurements in deposition hole DA3545G01. The vertical blue lines differentiate between periods of similar environmental conditions (see Table 4-1).

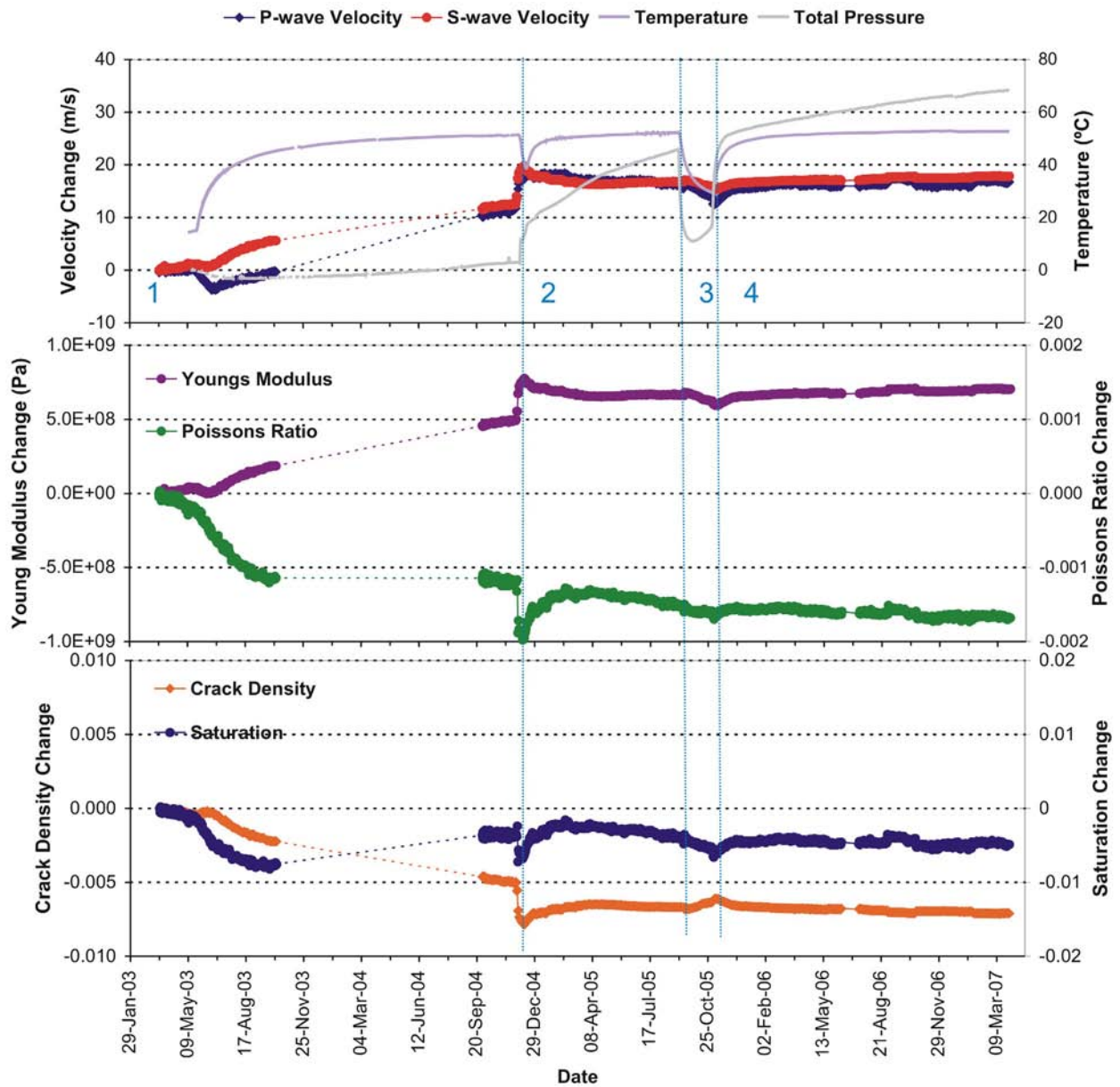


Figure 4-2: Average P- and S-wave velocity change for raypaths on category 'S1' together with temperature (TR6045) and total pressure (PB616) (top), Young's Modulus and Poisson's Ratio change (middle), and Crack Density and Saturation change (bottom).

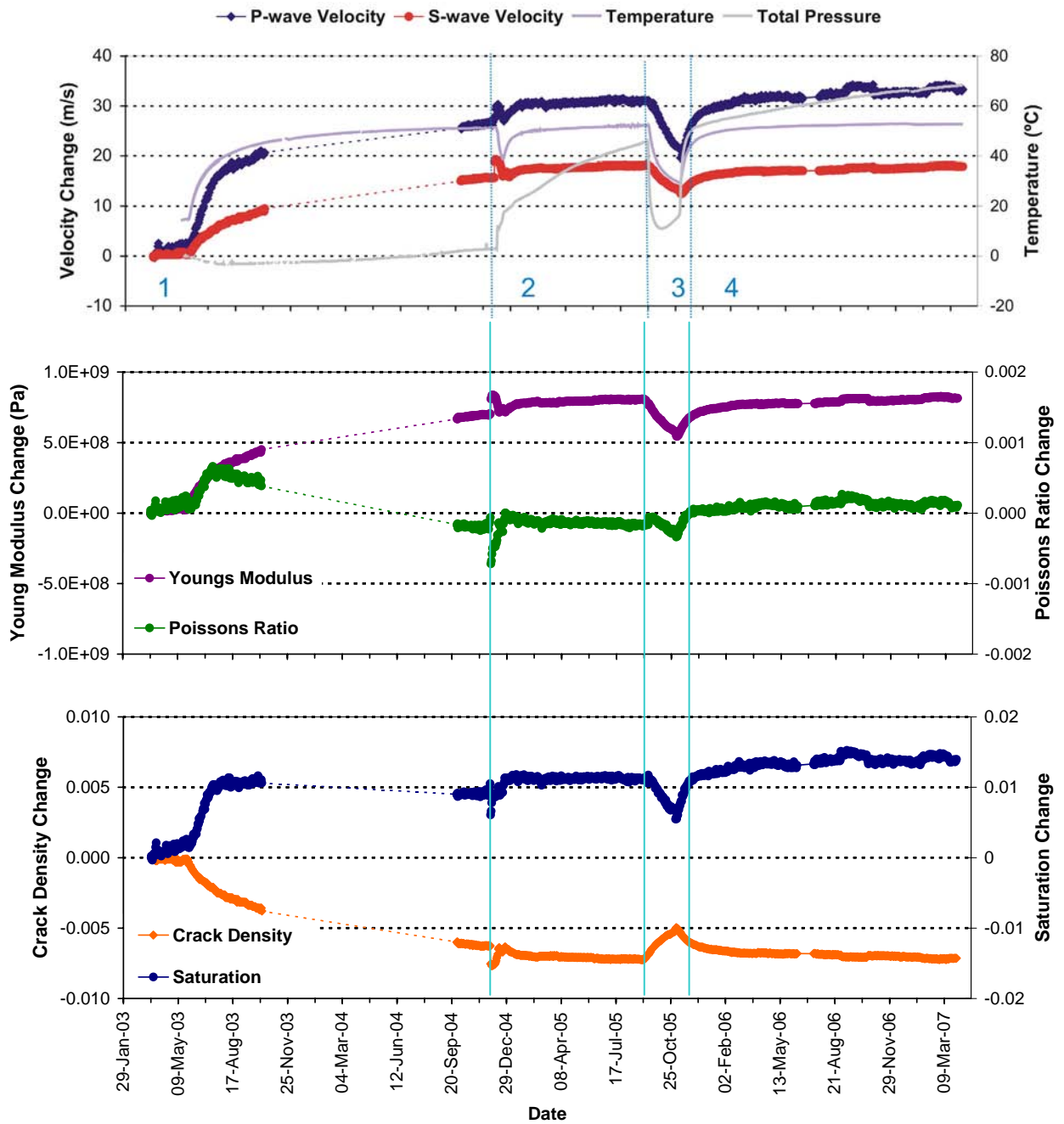


Figure 4-3: Average P- and S-wave velocity change for raypaths on category 'S3' together with temperature (TR6045) and total pressure (PB616) (top), Young's Modulus and Poisson's Ratio change (middle), and Crack Density and Saturation change (bottom).

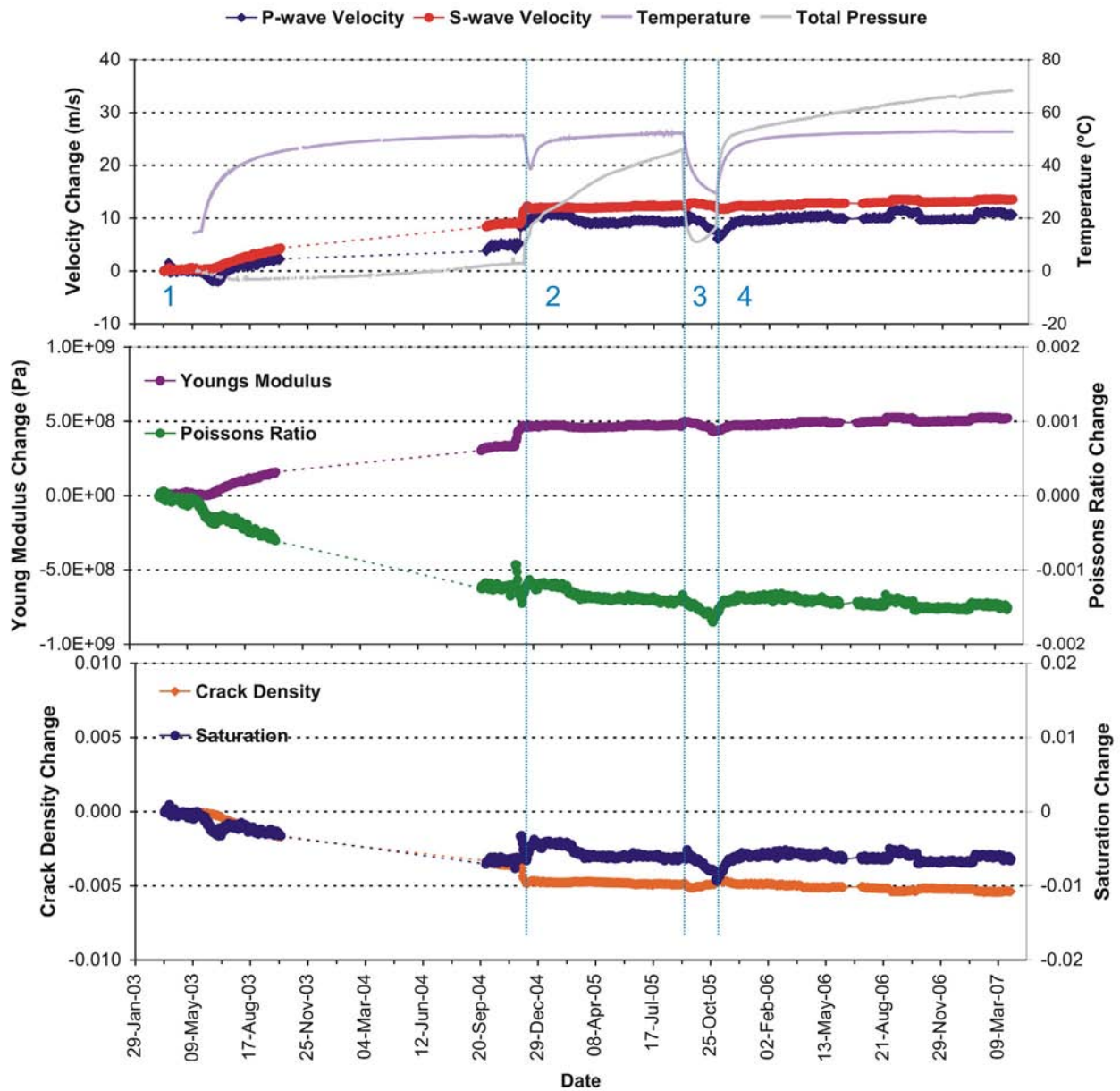


Figure 4-4: Average P- and S-wave velocity change for raypaths on category 'C1' together with temperature (TR6045) and total pressure (PB616) (top), Young's Modulus and Poisson's Ratio change (middle), and Crack Density and Saturation change (bottom).

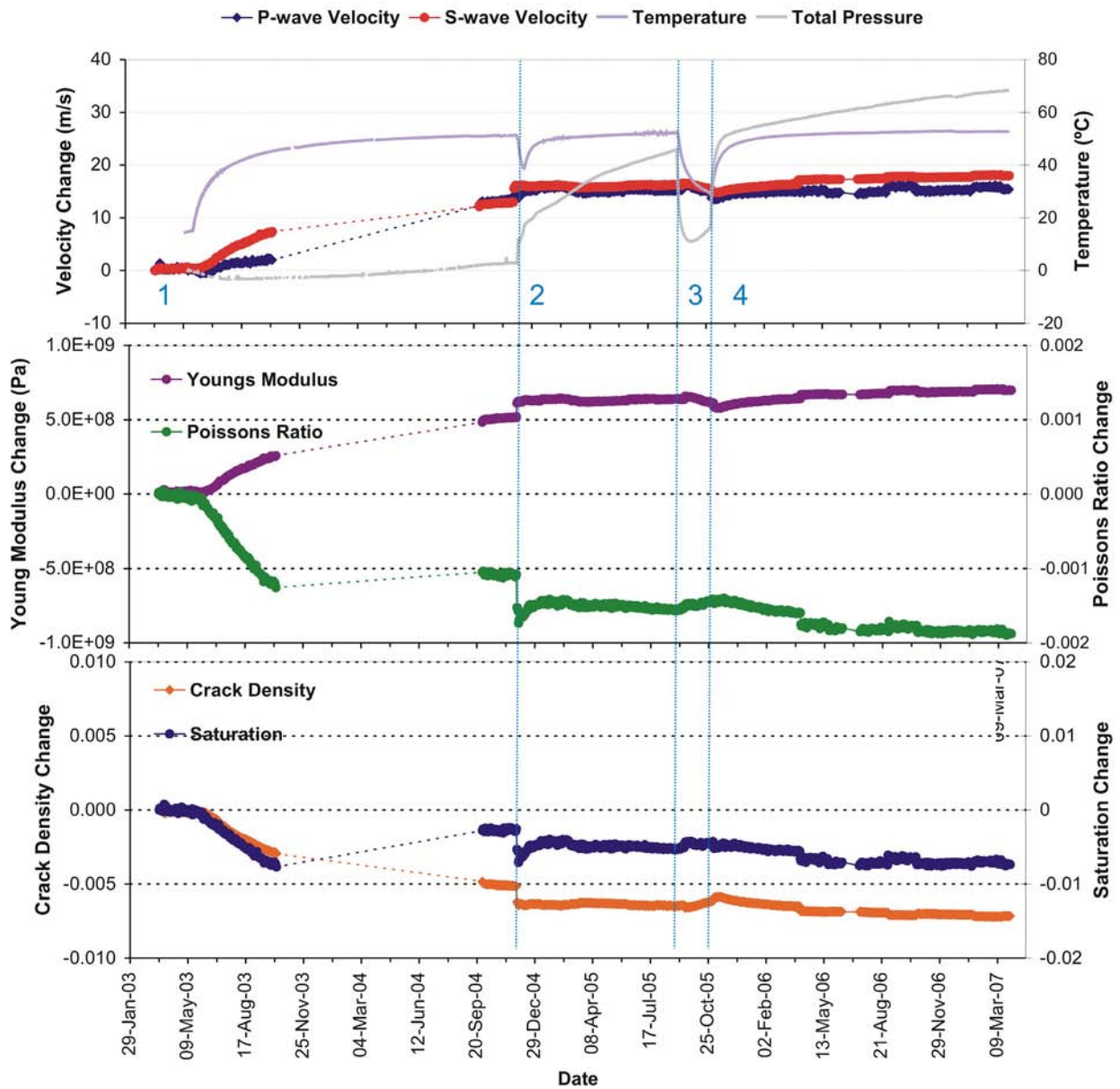


Figure 4-5: Average P- and S-wave velocity change for raypaths on category 'C2' together with temperature (TR6045) and total pressure (PB616) (top), Young's Modulus and Poisson's Ratio change (middle), and Crack Density and Saturation change (bottom).

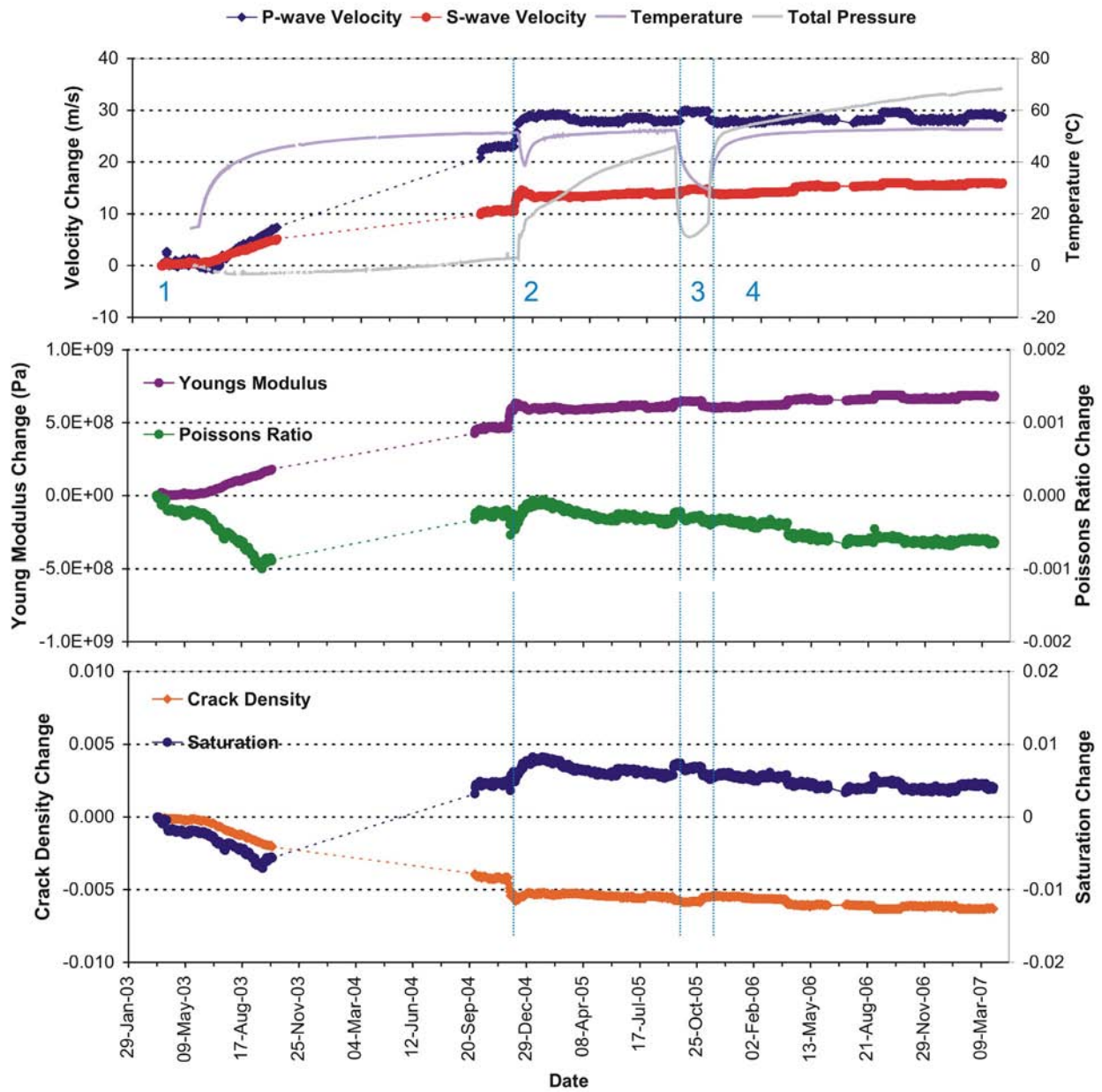


Figure 4-6: Average P- and S-wave velocity change for raypaths on category 'Far' together with temperature (TR6045) and total pressure (PB616) (top), Young's Modulus and Poisson's Ratio change (middle), and Crack Density and Saturation change (bottom).

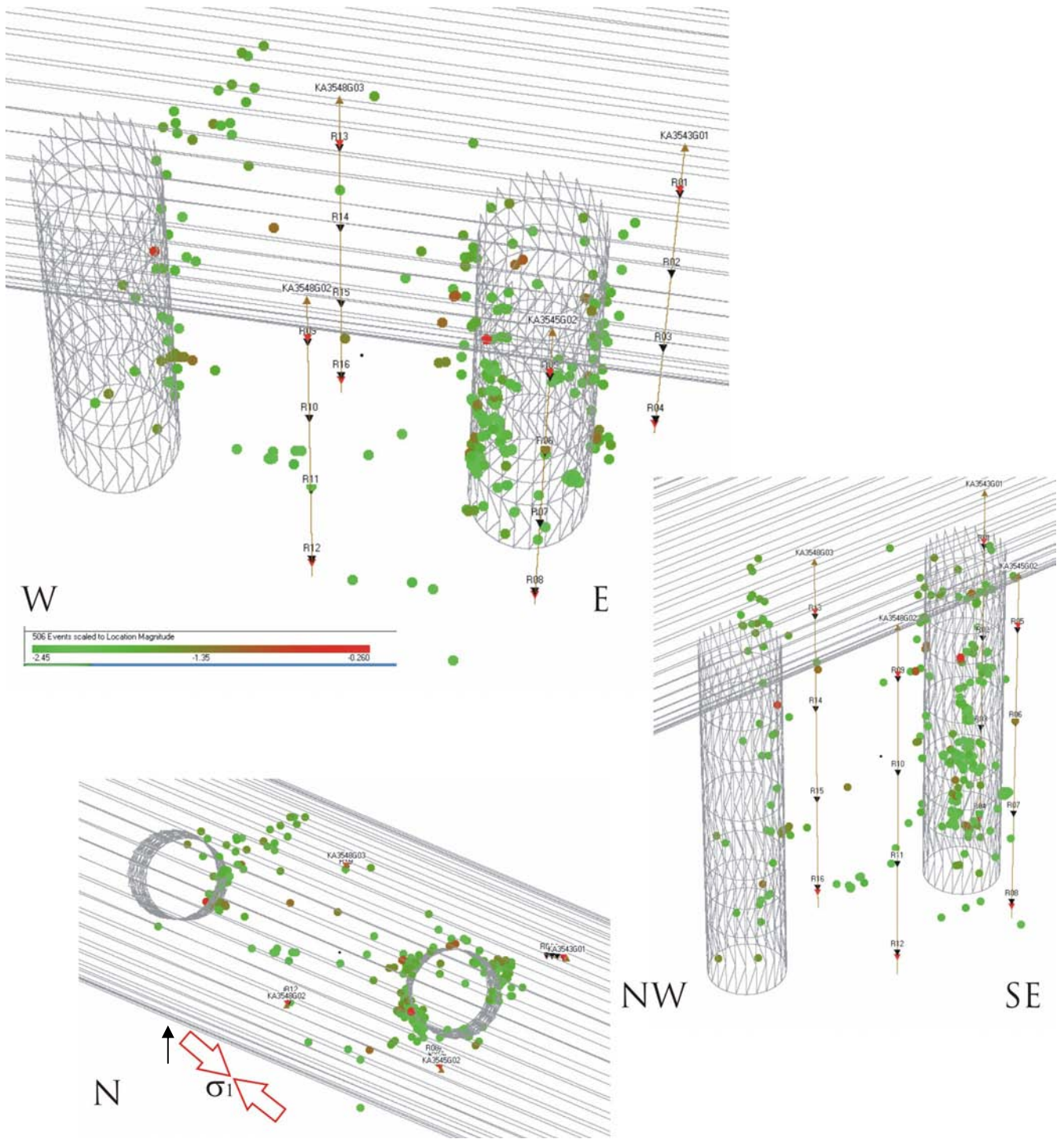


Figure 4-7: Projections of all AEs located during the heating phase (20th March 2003 to 31st March 2007). Events are scaled to location magnitude.

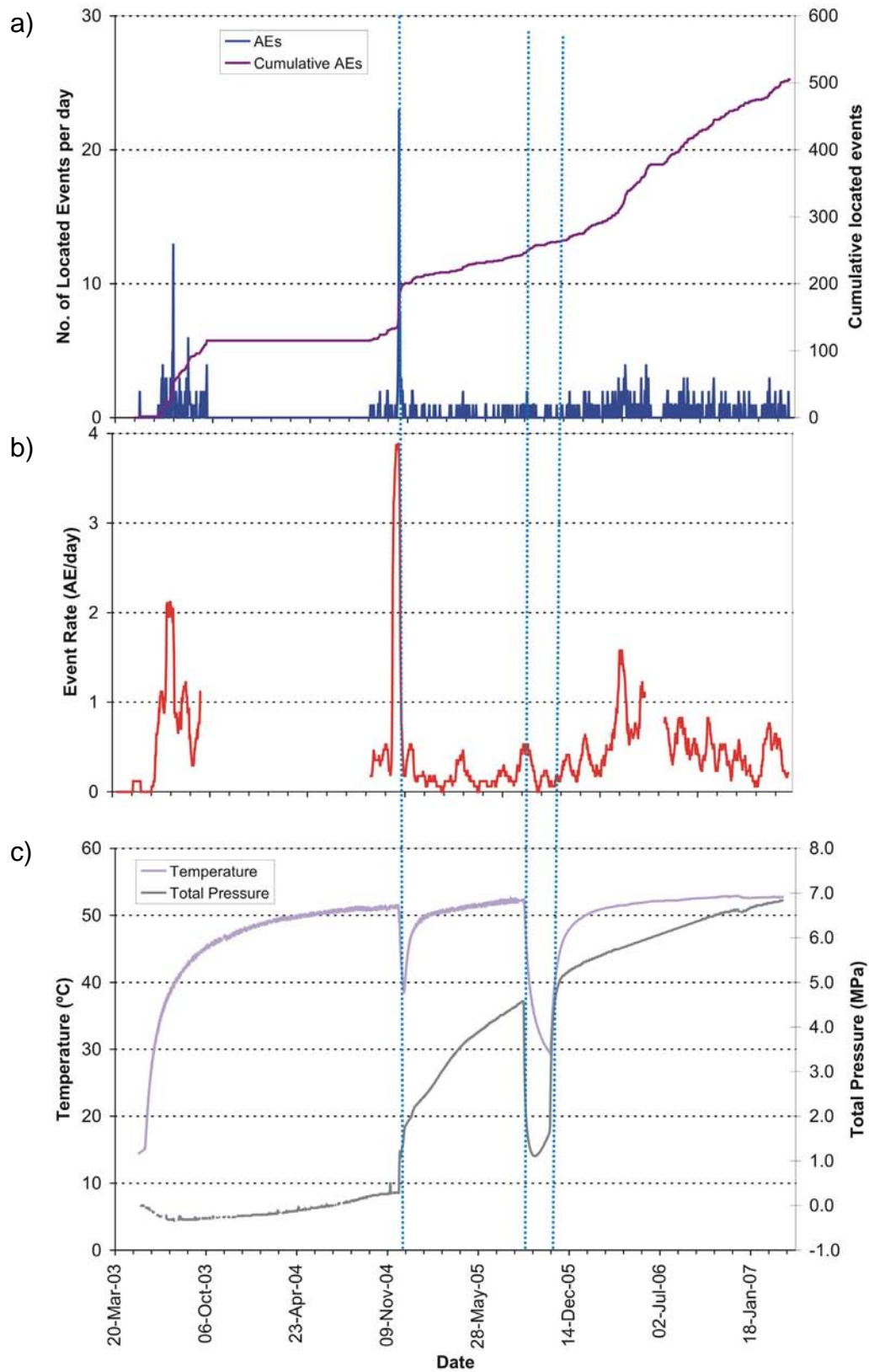


Figure 4-8: (a) Number and cumulative number of located events from the start of monitoring, (b) average number of AE events per day (averaged over 17 days) and (c) temperature (TR6045) and pressure (PB616) measurements in deposition hole DA3545G01.

PERIOD 1
25th May 2003 to
31st October 2004

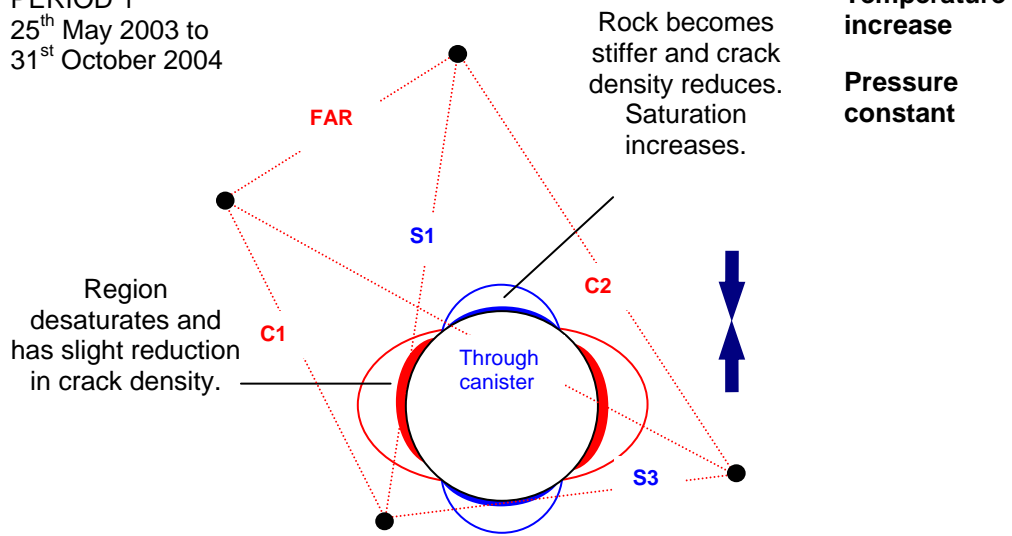


Figure 4-9: Schematic diagram of the deposition hole and explanation of changes experienced during Period 1.

PERIOD 2
1st November 2004 to
4th September 2004

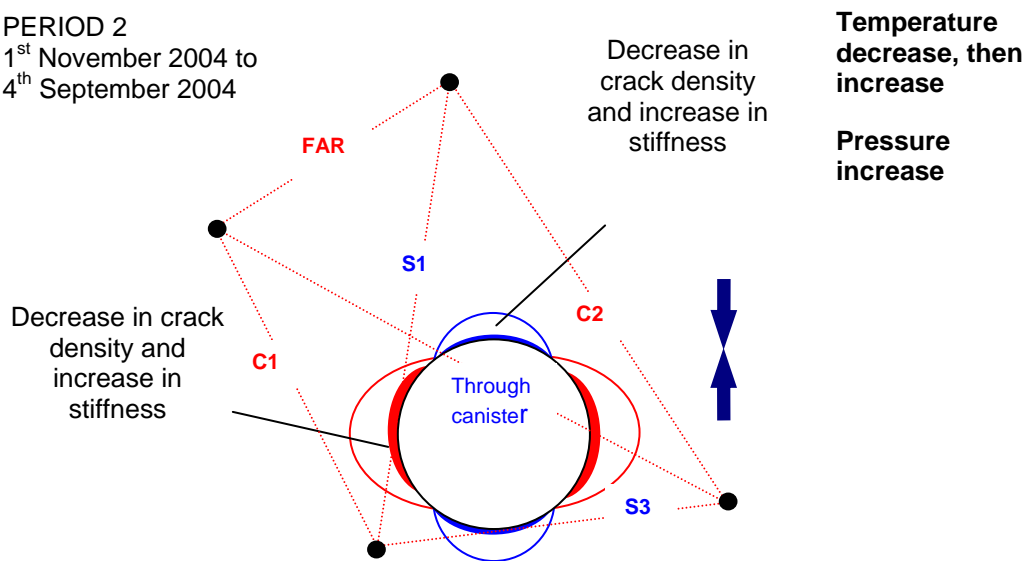


Figure 4-10: Schematic diagram of the deposition hole and explanation of changes experienced during Period 2.

PERIOD 35th
September 2005 to 2nd
November 2005

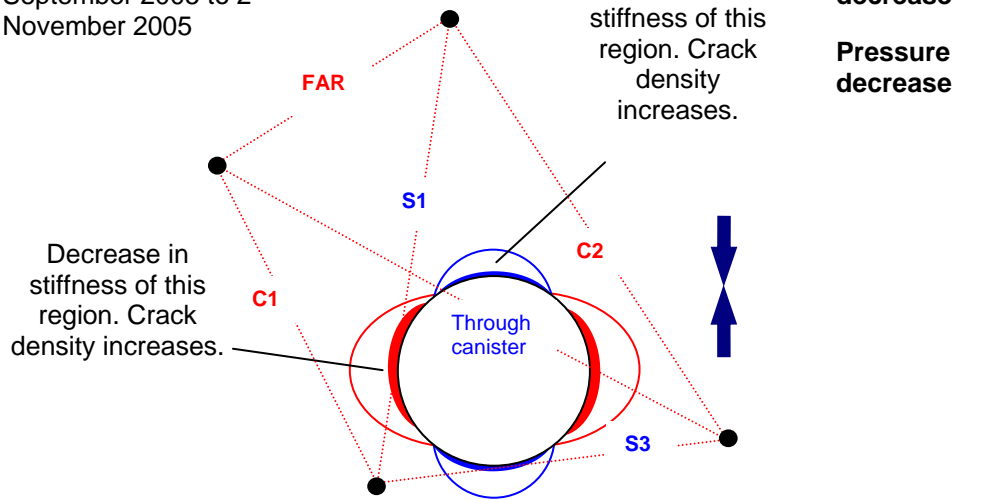


Figure 4-11: Schematic diagram of the deposition hole and explanation of changes experienced during Period 3.

PERIOD 43rd
November 2005 to
31st March 2007

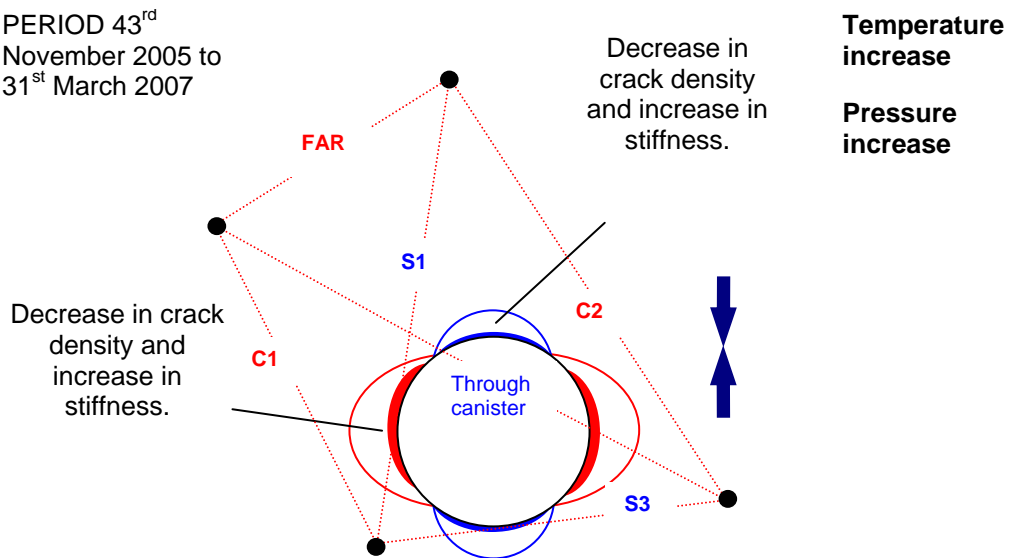


Figure 4-12: Schematic diagram of the deposition hole and explanation of changes experienced during Period 4.

References

Baker, C. and R.P. Young. 2002. Acoustic emission and ultrasonic monitoring around the TSX tunnel clay and concrete bulkheads between October 2001 and October 2002. Ontario Power Generation, Nuclear Waste Management Division Report.

Goudarzi, R. and L-E. Johannesson, Sensor Data Report (Period: 010917-061201). Prototype Repository. Report No: 16, International Progress Report IPR-07-05, Äspö Hard Rock Laboratory, Swedish Nuclear Fuel and Waste Management Company, Sweden, 2006.

Goudarzi, R., 2007. Pers. Comm.

Haycox, J.R., W.S. Pettitt, and R.P. Young, Acoustic Emission and Ultrasonic Monitoring During the Heating of Deposition hole DA3545G01 in the Prototype Repository to March 2005, International Progress Report IPR-05-30, Äspö Hard Rock Laboratory, Swedish Nuclear Fuel and Waste Management Company, Sweden, 2005a.

Haycox, J.R., W.S. Pettitt, and R.P. Young, Acoustic Emission and Ultrasonic Monitoring Results from Deposition Hole DA3545G01 in the Prototype Repository between April 2005 and September 2005, International Progress Report IPR-05-31, Äspö Hard Rock Laboratory, Swedish Nuclear Fuel and Waste Management Company, Sweden, 2005b.

Haycox, J.R., W.S. Pettitt, and R.P. Young, Acoustic Emission and Ultrasonic Monitoring Results from Deposition Hole DA3545G01 in the Prototype Repository between October 2005 and March 2006, International Progress Report IPR-06-23, Äspö Hard Rock Laboratory, Swedish Nuclear Fuel and Waste Management Company, Sweden, 2006a.

Haycox, J.R., W.S. Pettitt, and R.P. Young, Acoustic Emission and Ultrasonic Monitoring Results from Deposition Hole DA3545G01 in the Prototype Repository between April 2006 and September 2006, International Progress Report IPR-06-36, Äspö Hard Rock Laboratory, Swedish Nuclear Fuel and Waste Management Company, Sweden, 2006b.

Maxwell, S.C., and R.P. Young, A controlled in-situ investigation of the relationship between stress, velocity and induced seismicity, *Geophys. Res. Lett.*, 22, 1049-1052, 1995.

Patel, S., L.-O. Dahlstrom, and L. Stenberg, Characterisation of the Rock Mass in the Prototype Repository at Äspö HRL Stage 1, Äspö Hard Rock Laboratory Progress Report HRL-97-24, Swedish Nuclear Fuel and Waste Management Company, Sweden, 1997.

Pettitt, W.S., C. Baker, and R.P. Young, Acoustic emission and ultrasonic monitoring during the excavation of deposition holes in the Prototype Repository, International Progress Report IPR-01-01, Äspö Hard Rock Laboratory, Swedish Nuclear Fuel and Waste Management Company, Sweden, 1999.

Pettitt, W.S., C. Baker, and R.P. Young, Analysis of the in-situ principal stress field at the HRL using acoustic emission data, International Progress Report IPR-01-09, Äspö Hard Rock Laboratory, Swedish Nuclear Fuel and Waste Management Company, Sweden, 2000.

Pettitt, W.S., C. Baker, R.P. Young, L. Dahlstrom, and G. Ramqvist, The assessment of Damage Around Critical Engineering Structures Using Induced Seismicity and Ultrasonic Techniques, *Pure and Applied Geophysics*, 159, 179-195, 2002.

Pettitt, W.S., D.S. Collins, M.W. Hildyard, R.P. Young, C. Balland and P. Bigarré. 2004. An Ultrasonic Tool for Examining the Excavation Damaged Zone around Radioactive Waste Repositories – The OMNIBUS project, in *EC Euradwaste04 Conference*, Luxembourg.

Pettitt, W.S., Baker, C., Collins, D.S., and R.P. Young, 2005. InSite Seismic Processor – User Operations Manual Version 2.13. Applied Seismology Consultants Ltd., Shrewsbury, UK.

SKB, Äspö Hard Rock Laboratory: Current Research Projects 1998, Swedish Nuclear Fuel and Waste Management Company, Sweden, 1999.

Telford, W.M., Geldart, L.P., and Sheriff, R.E., *Applied Geophysics: Second Edition*, Cambridge University Press, 1990.

Young, R.P. and W.S. Pettitt, Investigating the stability of engineered structures using acoustic validation of numerical models, in *Geotechnical Special Publication No 102*, edited by J.F. Labuz, S.D. Glaser, and E. Dawson, pp. 1-15, ASCE, USA, 2000.

Zimmerman, R.W and M.S. King, Propagation of acoustic waves through cracked rock, 20th Symposium on Rock Mechanics, Rapid City, SD, 1985.

Appendix I Previous Monitoring at the Prototype Repository

Ultrasonic monitoring has been conducted at the Prototype Repository in some form since September 1999. During excavation, monitoring of both deposition holes in Tunnel Section 2 (DA3551G01 and DA3545G01) was undertaken to delineate zones of stress related fracturing and quantitatively measure fracturing in the damaged zone [Pettitt *et al.*, 1999]. Thereafter, monitoring has been undertaken on a single deposition hole (DA3545G01), and the response of the surrounding rock to changes in temperature and pressure has been measured (see Table 4.3). The report by Haycox *et al.*[2005a] presented results from the initial heating Haycox *et al.*[2005b] was the first of an ongoing 6-monthly processing and interpretation of the results. This report presents new results from the period 1st October 2006 to 31st March 2007.

Table 4-3: Summary of ultrasonic monitoring at the Prototype Repository to-date. Response Periods are defined in Haycox *et al.*[2006a].

Report	Monitoring Period	Location	Response Period
Pettitt <i>et al.</i> [1999]	25/08/1999 to 18/09/1999	DA3551G01 and DA3545G01	Excavation
Haycox <i>et al.</i> [2005a]	20/03/2003 to 09/10/2003	DA3545G01	1
	29/04/2004 to 31/03/2005	DA3545G01	1, 2
Haycox <i>et al.</i> [2005b]	01/04/2005 to 30/09/2005	DA3545G01	2, 3
Haycox <i>et al.</i> [2006a]	01/10/2005 to 31/03/2006	DA3545G01	3, 4
Haycox <i>et al.</i> [2006b]	01/04/2006 to 30/09/2006	DA3545G01	4
Zolezzi <i>et al.</i> [2007]	01/10/2006 to 31/03/2007	DA3545G01	4

A temporary ultrasonic array was installed around the rock volume when deposition hole DA3545G01 and its neighbour DA3551G01 were first excavated in September 1999 [Pettitt *et al.*, 1999]. A total of 2467 AE triggers were obtained during monitoring of the two deposition holes. Of these 1153 were located. There was significantly more AE activity around the second deposition hole (labelled DA3545G01) than the first (DA3551G01). This difference is likely to depend upon intersection of the excavation with a greater number of pre-existing fractures. These fractures may be preferentially located in the side wall of the deposition hole or preferentially orientated to the *in situ* stress field. Fracturing associated with excavation-induced stresses was observed with AEs distributed mainly in regions orthogonal to the maximum principal stress, σ_1 . This was consistent with observations from the Canister Retrieval Tunnel and from dynamic numerical models. AEs, and hence microcrack damage, were shown to locate in clusters down the deposition hole and not as a continuous 'thin skin'. Pettitt *et*

al.[2000] showed that these clusters were associated with weaknesses in the rock mass generated by excavation through pre-existing fractures. Damage in the side wall of the deposition holes depended significantly on these pre-existing features. The *in situ* stress field was a contributing factor in that induced stresses were sufficiently high to create damage in these weakened regions although not sufficiently high to create significant damage in the rock mass as a whole.

A permanent ultrasonic array, with transducers grouted into instrumentation boreholes, was installed in the rock mass in June 2002. In this arrangement, ultrasonic monitoring has been conducted between 20th March and 9th October 2003, and then from 29th September 2004 to the present. A gap in monitoring occurred when the ultrasonic acquisition system was used for another experiment in the HRL (Pillar Stability Experiment). Processing and reporting of results has been undertaken by *Haycox et al.*[2005a], *Haycox et al.*[2005b], *Haycox et al.*[2006a] and *Haycox et al.*[2006b] and is further discussed in Section 4.2. A description of instruments measuring other environmental factors (such as temperature and pressure) and their locations can be found in *Goudarzi and Johannesson*[2007].

Appendix II Methodology

Data Acquisition

The ultrasonic array consists of twenty-four ultrasonic transducers configured as eight transmitters and sixteen receivers installed into four instrumentation boreholes. The transducers are fixed into the boreholes using specially designed frames (Figure 4-13) – two transmitters and four receivers per frame. The boreholes are vertical, 76mm in diameter and approximately 10 meters in length distributed around each deposition hole volume. The array has been designed so as to provide good coverage for AE locations and to provide ‘skimming’ ray paths that pass within a few centimetres of the deposition-hole wall. The layout of the instrumentation boreholes is shown in Figure 4-14 and described further in Table 4-4. Each of the ultrasonic transducers has a hemispherical brass cap fixed over its active face and is then spring-loaded against the borehole surface so as to obtain good coupling to the rock mass. The boreholes have then been filled with a slightly expansive grout so as to permanently fix the transducers in place, reduce the likelihood of damage to the transducers and to remove the borehole voids.

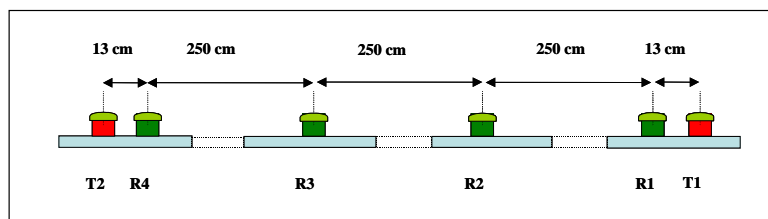


Figure 4-13: Top: Schematic diagram of the locations of all transducers on a single frame. Left: Photo of a section of the transducer assembly. Right: The transducer assembly during installation.

The piezoelectric transducers operate by converting a transient elastic wave into an electric signal or visa versa. The monitoring system is then operated in one of two modes. The first is used to passively monitor AE activity preferentially within the array volume. AEs release elastic energy in the same way as 'earthquakes' but over a very small scale. At these frequencies AEs have a moment magnitude (M_w) of approximately -6. They occur either during the creation process of new fractures within the medium, or on pre-existing fractures due to small scale movements. Each receiver has a frequency response of approximately 35-350kHz and contains a 40dB pre-amplifier. This minimises a reduction in signal-to-noise between the sensors and the acquisition system. The sensors have a vulcanised surround and a high pressure reinforced cable to protect them from water infiltration. In addition, polyamide tubes and *Swagelok* connectors have been fitted to the cables to reduce the likelihood of breakage.

Figure 4-15 shows a schematic diagram of the acquisition system used. Cables from each transducer pass through the pillar between the PRT and the G-tunnel. Data acquisition uses a Hyperion Ultrasonic System controlled by a PC, set up within a cabin provided by SKB. This has 16 receiving channels and 8 transmitting channels. An AE is recorded when the amplitude of the signal on a specified number of channels exceeds a trigger threshold within a time window of 5ms. The system then records the full-waveform signals from all 16 transducers. In this case a trigger threshold of 50mV on three channels was used. This allows the system to have sufficient sensitivity to record high quality data without recording an abundance of activity that cannot be processed due to very small signal to noise on only a few channels. The captured signals are digitised with a sampling interval of 1 μ s and a total length of 4096 data points. In general, low noise levels were observed (<2mV) giving high signal to noise and good quality data. AE monitoring is set to switch off during daytime working hours (6am-8pm) so as to minimise the amount of noise recorded from human activity.

A second operating mode actively acquires ultrasonic waveforms by scanning across the volume. This allows measurements of P- and S-wave velocities and signal amplitudes over a possible 128 different ray paths. By repeating these ultrasonic surveys at increments in time, a temporal analysis is obtained for the variation in medium properties. Ultrasonic surveys are conducted daily at 1am in order to measure changes in P- and S-wave signals. At that time of night, no human activity will cause noise that can interfere with the signals received. A Panametrics signal generator is used to produce a high frequency electric spike. This is sent to each of the 8 transmitters in turn. The signal emitted from each transmitter is recorded over the 16 receivers in a similar fashion to that described above. An external trigger pulse from the signal generator is used to trigger the acquisition system and identifies the transmission start time to an accuracy of one sample point. In order to decrease random noise the signal from each transmitter is stacked 100 times.

Table 4-4: Boreholes used for AE monitoring of deposition hole DA3545G01.

SKB Borehole designation	ASC Borehole reference	Transducer Numbers
KA3543G01	1	T1, T2, R1-R4
KA3545G02	2	T3, T4, R5-R8
KA3548G03	3	T5, T6, R9-R12
KA3548G02	4	T7, T8, R13-R16

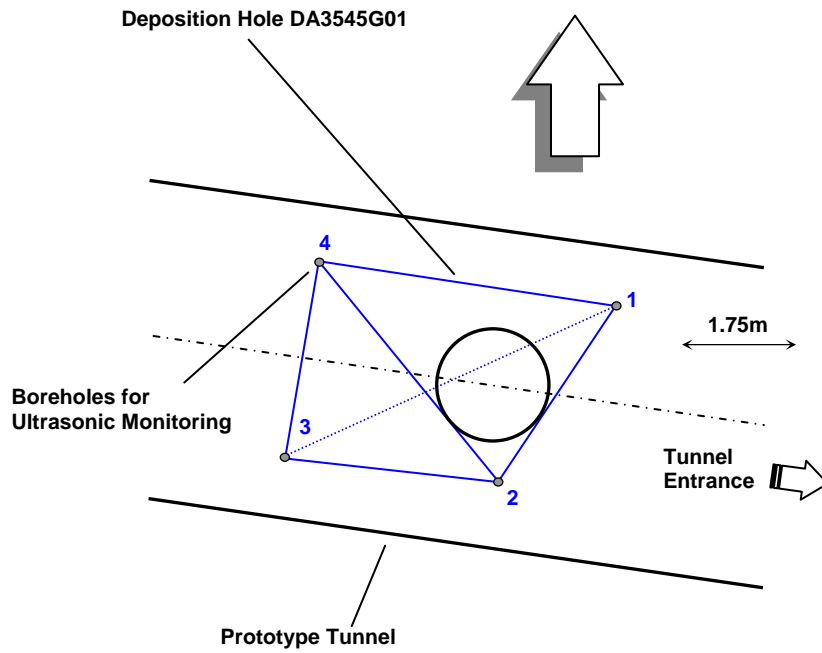


Figure 4-14: Plan view of the array geometry for Deposition Hole DA3545G01 during heating in the Prototype Tunnel. The blue solid lines represent direct raypaths between sondes illustrating their ‘skimming’ nature. The blue dashed line represents a raypath that travels through the deposition hole.

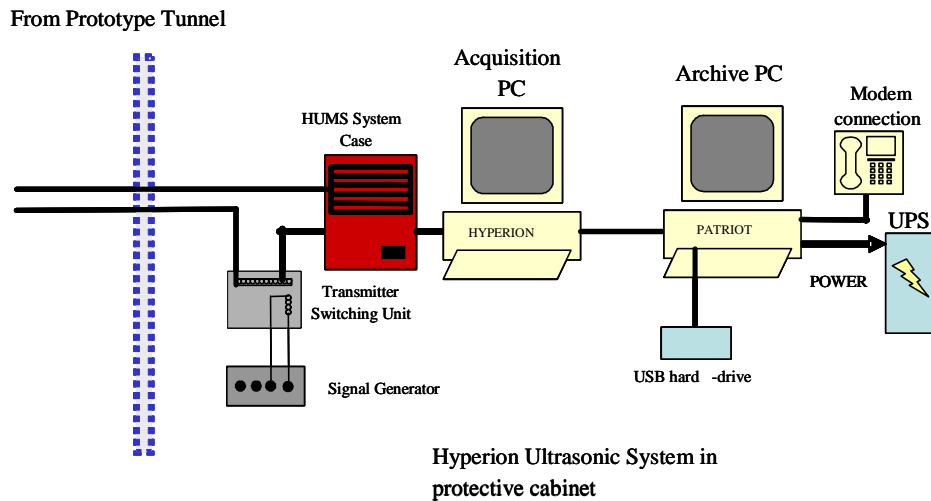


Figure 4-15: Schematic diagram of the hardware used for the heating stage in the Prototype Repository. The ultrasonic pulse generator sends a signal to each transmitter and the resulting signal is recorded on each receiver. The receivers are also used to listen for AE activity. The archive PC is required to make a copy of the data for backup purposes.

Processing Procedure

Overview

ASC's InSite Seismic Processor has been used to automatically process both the AE and ultrasonic survey data. Appendix IIIA and Appendix IIIB give the processing parameters used. *Pettitt et al.*[2005] provides a detailed description of this software.

Ultrasonic Data Procedure

The ultrasonic survey full-waveform data was initially stored with the AE data. This was automatically sorted and the survey data extracted to a separate processing project. A 'reference' survey from the previous monitoring period was used, and imported into the project. The P- and S-wave arrivals were manually picked during the previous monitoring period. Knowing the transmitter and receiver locations, the ultrasonic velocity for each ray path was calculated with an estimated uncertainty of $\pm 30 \text{m.s}^{-1}$ (± 3 data points). A cross-correlation procedure was then used to automatically process subsequent surveys. This technique cross-correlates P- and S-wave arrivals from a transmitter-receiver pair with arrivals recorded on the same transmitter-receiver pair on the reference survey. This results in high-precision measurements of P- and S-wave velocity change with estimated uncertainties of $\pm 2 \text{m.s}^{-1}$ between surveys. Note that when the transmitter and receiver are on the same borehole, the raypath is not used due to the introduction of transmission effects from the instrumentation borehole, grout and transducer frames.

The main reason for the reduction of uncertainty when using the cross-correlation procedure is the dependency of manual picking on the user's judgement of the point of arrival. This can usually be quite indiscriminate because of random noise superimposed on the first few data points of the first break. Additionally, the procedure is run automatically without any loss of precision resulting in efficient waveform processing. The cross-correlation procedure then allows for a high-resolution analysis to be performed and hence small changes in velocity to be observed. This is extremely important when changes in rock properties occur over only a small section (5%) of the ray path.

Figure 4-16 gives example waveforms recorded from one of the transmitters during this reporting period. Each waveform is first automatically picked to obtain an estimate of the P-wave or S-wave arrival. A window is then automatically defined around the arrival and a bell function is applied, centred on the automatic pick. The data at the ends of the window then have a much smaller effect on the cross-correlation. The windowed data is then cross-correlated [*Telford et al.*, 1990] with a similar window constructed around the arrival on the reference survey. The change in arrival time is then converted to a change in velocity knowing the manually-picked arrival time for the reference survey. Waveforms that do not provide automatic picks are not cross-correlated. This gives an automatic discrimination of signals that have very poor signal to noise ratios and could give spurious cross-correlation results from poor discrimination of the first arrival. During the automatic processing an arrival amplitude is also calculated from within a processing window defined by a minimum and maximum transmission velocity. This provides a robust measure of arrival amplitudes between surveys.

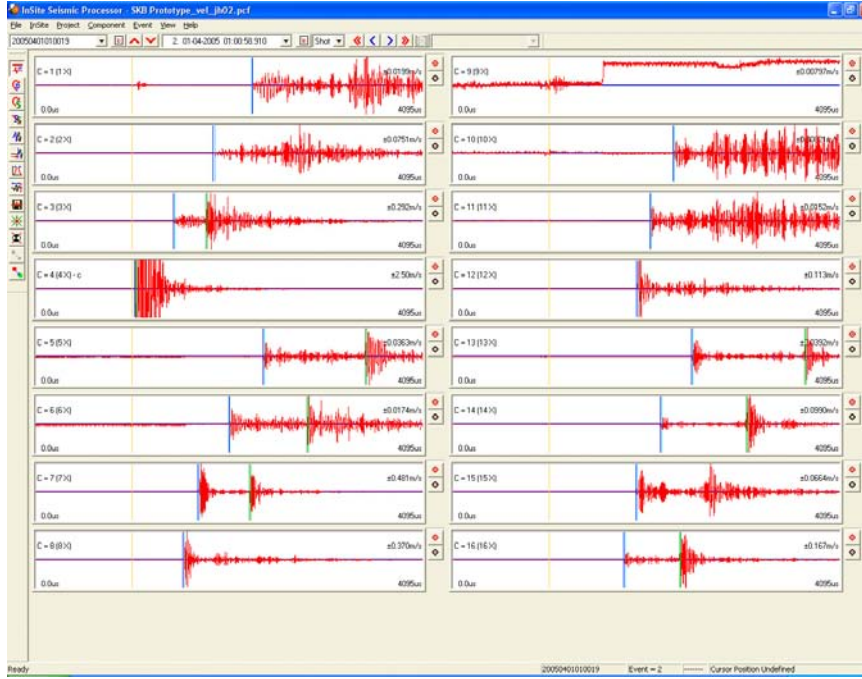


Figure 4-16: Waveforms recorded from one transmitter on the array of sixteen receivers. The gold markers indicate the transmission time. The blue and green markers indicate picked P- and S-wave arrivals respectively.

When calculating average velocities and amplitudes, raypaths passing through the deposition hole are removed due to the uncertain transmission paths produced by the wave travelling in the rock around the deposition hole and through the bentonite, fluid and canister fill. Therefore the majority of raypaths between boreholes 1 and 3 (transmitters 1, 2, 5, 6 and receivers 1, 2, 3, 4) are not used in the analysis. An exception is made for the deepest raypaths that pass under the deposition hole entirely through rock.

The dynamic Young's modulus E , and dynamic Poisson's Ratio, ν , can be calculated from the velocity measurements using Equation 1 and Equation 2

$$E = \rho V_s^2 \left(\frac{3V_P^2 - 4V_S^2}{V_P^2 - V_S^2} \right) \quad \text{Equation 1}$$

$$\nu = \frac{V_P^2 - 2V_S^2}{2(V_P^2 - V_S^2)} \quad \text{Equation 1}$$

V_P and V_S values are also used to model for crack density (c) and saturation (s) in the rock mass using the method of *Zimmerman and King*[1985]. The crack density parameter is defined by the number of cracks (penny-shaped) per unit volume multiplied by the mean value of the cube of the crack radius (Equation 3). This method assumes the elastic modulus E and ν in the damaged material normalized to the undisturbed material, decrease exponentially with crack density. Also assumed are the shear modulus (μ) is unaffected by s , and the bulk modulus (k) increases linearly with s , equalling that of uncracked rock when $s=1$. Equation 4 shows the calculation used to determine saturation.

$$c = \frac{9}{16} \ln \left(\frac{2\mu}{E_0 - 2\mu\nu_0} \right) \quad \text{Equation 3}$$

$$s = \frac{k(c,s) - k(c,0)}{k_0 - k(c,0)} \quad \text{Equation 3}$$

The calculations require an estimation of the completely undisturbed rock (i.e. an unsaturated, uncracked, intact rock mass). This study assumes values of $V_{OP} = 6660 \text{m.s}^{-1}$, and $V_{OS} = 3840 \text{m.s}^{-1}$ for the undisturbed material taken from laboratory tests on a similar granite, summarized in *Maxwell and Young*[1995]. A value of 2650 kg m^{-3} is presented by *Pettitt et al.*[2002] for the density of the rock mass.

The calculations of Young's Modulus and Poisson's ratio from measured velocities makes an assumption of an isotropic elastic medium. Under this assumption a rock can be completely characterised by two independent constants. One case of an isotropic elastic medium is a rock with a random distribution of cracks embedded in an isotropic mineral matrix. Under the application of a hydrostatic compressive stress, the rock will stay isotropic but become stiffer (which will become characterised by increased velocity V_P , V_S and therefore increased Young's modulus). In contrast, under the application of a uniaxial compressive stress, cracks with normals parallel or nearly parallel to the applied stress will preferentially close and the rock will take on a transversely isotropic symmetry. Under this situation P- and S-wave velocities become variable with orientation. The crack density and saturation calculations also assume an isotropic elastic medium.

It should be noted that E and ν calculated in this report are dynamic measurements due to the small strains exerted on the rockmass at high frequencies from the passing ultrasonic waves. Static E and ν measurements, made from uniaxial laboratory tests on rock samples, may be different from dynamic values – even if sample disturbance is minimal – due to the larger strains exerted over relatively long periods of time.

Acoustic Emission Procedure

The procedure used to process the AEs in this reporting period has been undertaken as follows:

1. Calibration surveys from the installation phase (when the deposition hole was open) have been used to optimise an automatic picking and source location algorithm and check location uncertainties. ASC's InSite seismic processing software was used for location and visualisation.
2. Where possible, P- and S-wave arrival times were measured for each AE using the automatic picking procedure.
3. AEs with ≥ 6 P-wave arrival times were input into a downhill-simplex location algorithm [*Pettitt et al.*, 2005]. This has the option of incorporating either a three-dimensional anisotropic velocity structure or an isotropic structure. Velocities calculated from the ultrasonic surveys were used.

4. The waveforms from all events were visually inspected to ensure they were ‘real’ acoustic emissions. Events were removed if they had the appearance of noise spikes (increase in amplitude is recorded on all channels at the same time) or they were the result of human noise (long period events that occur at close intervals during the day).
5. The acoustic emissions that remained had their arrivals manually picked to obtain the best possible location. Any events that located outside the expected region of activity were further checked to ensure accuracy. Experience from previous studies around deposition holes showed that large source location errors were produced if significant portions of a ray path passed through the excavated deposition hole void. This only becomes a problem for the largest AEs. AEs were reprocessed with these ray paths removed.
6. Finally, a filter was applied to remove all AEs with a location error greater than 1.0.

During the equipment installation phase, calibration shots have been undertaken to assess the sensitivity of the system to ‘real’ AEs and to determine the accuracy with which real events could be subsequently located by the array of sensors. A series of test ‘shots’ were performed on the wall of deposition hole DA3545G01 (Figure 4-17). The shots consisted of undertaking 10 ‘pencil lead breaks’ and 10 hits with a screw-driver at 1 metre intervals down 4 lines along the deposition hole wall. The pencil-lead tests involved breaking the 0.5 mm lead from a mechanical pencil against the borehole wall. This is a ‘standard’ analogue for an AE as it generates a similar amount of high-frequency energy. An example of a pencil lead break test is shown in Figure 4-18. This was made at 6 metres below the tunnel surface on the deposition hole wall at a point adjacent to borehole KA3548G02. This corresponds to an AE source dimension on the millimetre scale (grain size).

The screw-driver hits provided a good amplitude signal for assessing the accuracy with which events can be located within the volume surrounded by the array. Figure 4-17 shows the results from one processed set of locations for a line of shots down the deposition hole wall. This shows that the array is able to locate events with good accuracy and consistency within an estimated uncertainty of approximately 10cm.

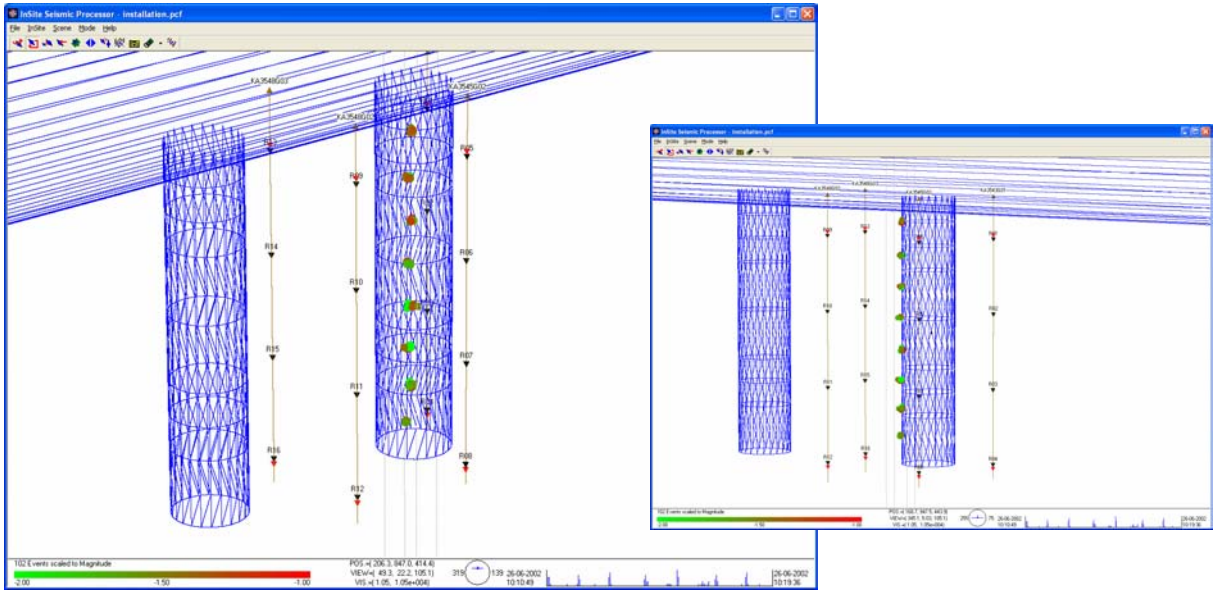


Figure 4-17: Locations of calibration shots obtained from a series of tests at 1 metre intervals down the wall of deposition hole DA3545G01. The two views show that these line up and are located close to the surface of the hole.

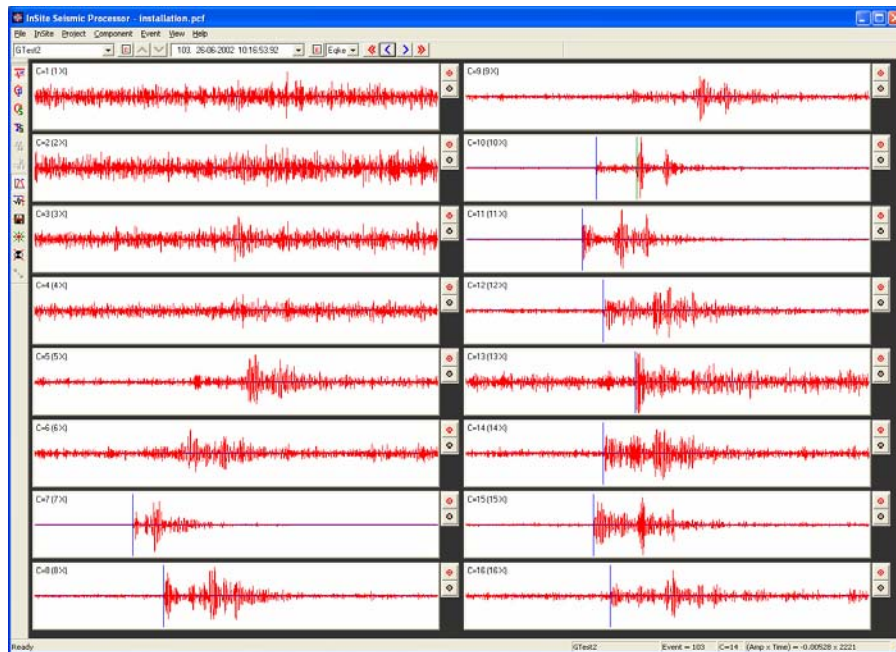


Figure 4-18: Example waveforms from each of the 16 receiving channels for a ‘pencil-lead break’ test undertaken against the Deposition Hole (DA3545G01) wall 6 metres below the tunnel floor.

Appendix III Processing Parameters

A: Ultrasonic survey processing parameters:

PROCESSING PARAMETERS

Velocity survey processing

EVENT INITIALISATION	
View/process waveforms by	Channel
Channel-view Width-to-height ratio	6
Waveform Response type	Set from sensor
Sampling time	1
Time units	Microseconds
Pre-signal points	200
Spline sampling time	0.2
Waveform To point	1023
P-Time correction	0
S-Time correction	0
Automatically update Channel Settings	NOT SET
Project Files	NULL

AUTO PICKING	
Allow P-wave-autopicking	YES, Use first peak in the auto-pick function
Back-window length	100
Front-window length	35
Picking Threshold	4
Min. Peak-to-Peak amplitude	0
Allow S-Wave Autopicking	YES, Use first peak in the auto-pick function
Back-window length	100
Front-window length	35
Picking Threshold	3
Min. Peak-to-Peak amplitude	0
Allow Automatic Amplitude Picking	YES
Use Velocity Window Picking	YES
P-wave Min. Velocity/Max. Velocity	4500, 6500
S-wave Min. Velocity/Max. Velocity	2500, 3500

CROSS-CORRELATION	
CCR Events	Referenced to a Survey
Reference Component	20041208005920
Reference Event	NULL
Window construction method	Front to Back
Window comparison method	Fixed to reference picks
Window Parameters	Back-window length = 20 Front-window length=30 Rise-time multiplier = NULL Power to raise waveform =1 Split to a Spline function = YES Obtain absolute waveform= NOT SET

LOCATER	<i>(not used in velocity surveys)</i>
Method	SIMPLEX INTO GEIGER
Method settings Simplex settings Geiger settings	Tolerance = 0.01 LPNorm = 1 P-wave weighting = 1 S-wave weighting = 1 Use Outlier Identification = NOT SET Arrival error factor = x2 Tolerance (Loc. units) = 0.01 Step size (Loc.units) = 0.1 Max. Iterations = 100 Conditional No. Limit = 1000000000
Velocity Structure	Homogeneous Isotropic
Velocity Structure settings	P-wave velocity = 6000 m.s ⁻¹ S-wave velocity = 3350 m.s ⁻¹ Attenuation = 200 Q(S) value = 100
Data to use	P-wave Arrivals Only
Distance units	Metres
Working time units	Microseconds
Min P-wave arrivals	0
Min S-wave arrivals	0
Min Independent arrivals	5
Max. Residual	20
Start point	Start at the centroid of the array
Write report to RPT	NOT SET
Source parameters	Set to calculate automatically

B: AE processing parameters:

PROCESSING PARAMETERS

AE processing

EVENT INITIALISATION	
View/process waveforms by	Channel
Channel-view Width-to-height ratio	6
Waveform Response type	Set from sensor
Sampling time	1
Time units	Microseconds
Pre-signal points	200
Spline sampling time	0.2
Waveform To point	1023
P-Time correction	0
S-Time correction	0
Automatically update Channel Settings	SET
Project Files	NULL

AUTO PICKING	
Allow P-wave-autopicking	YES, Use max peak in the auto-pick function
Back-window length	100
Front-window length	35
Picking Threshold	5
Min. Peak-to-Peak amplitude	0
Allow S-Wave Autopicking	YES, Use max peak in the auto-pick function
Back-window length	100
Front-window length	35
Picking Threshold	5
Min. Peak-to-Peak amplitude	0
Allow Automatic Amplitude Picking	NOT SET
Use Velocity Window Picking	YES
P-wave Min. Velocity/Max. Velocity	4500, 6500
S-wave Min. Velocity/Max. Velocity	2500, 3500

CROSS-CORRELATION	<i>(not used in AE processing)</i>
CCR Events	NOT SET
Reference Component	NOT SET
Reference Event	NULL (not activated)
Window construction method	Individual
Window comparison method	Fixed to reference picks
Window Parameters	Back-window length = 20 Front-window length = 30 Rise-time multiplier = NULL Power to raise waveform = 1 Split to a Spline function = NOT SET Obtain absolute waveform = NOT SET

LOCATER	
Method	SIMPLEX INTO GEIGER
Method settings Simplex settings Geiger settings	Tolerance = 0.01 LPNorm = 1 P-wave weighting = 1 S-wave weighting = 1 Use Outlier Identification = NOT SET Arrival error factor = x2 Tolerance (Loc. units) = 0.01 Step size (Loc.units) = 0.1 Max. Iterations = 100 Conditional No. Limit = 1000000000
Velocity Structure	Homogeneous Isotropic
Velocity Structure settings	P-wave velocity = 5983 m.s ⁻¹ S-wave velocity = 3343 m.s ⁻¹ Attenuation = 200 Q(S) value = 100
Data to use	P-wave Arrivals Only
Distance units	Metres
Working time units	Microseconds
Min P-wave arrivals	0
Min S-wave arrivals	0
Min Independent arrivals	5
Max. Residual	20
Start point	Start at the centroid of the array
Write report to RPT	NOT SET
Source parameters	Set to calculate automatically

EVENT FILTER	
Date and Time	NOT SET
Location volume	Minimum = (235, 880, 420)
	Maximum = (300, 964, 463)
L. Magnitude	NOT SET
Location Error	1
Independent Instruments	Minimum = 0

SOURCE PARAMETERS	
Automatic source-parameter windows	P-wave back window = 10
	P-wave front window = 50
	S-wave back window = 10
	S-wave front window = 50
Source parameter calculations	Min number to use = 3
Automatic source-parameter windows	Apply Q correction = SET
	Source density = 2640
	Source shear modulus = 39131400000
	Av. radiation coefficient: $F_p = 0.52$, $F_s = 0.63$
Source parameter calculations	Source coefficient: $k_p = 2.01$, $k_s = 1.32$
Magnitude calculations	Instrument magnitude = $1 * \log(\text{ppV}) + 0$
	Moment magnitude = $0.666667 * \log(M_0) + -6$

